

Environmental Controls on Observed Spatial Variability of Soil Pore Water Geochemistry in Small Headwater Catchments Underlain with Permafrost

Nathan Alec Conroy,^{1*} Jeffrey M. Heikoop,¹ Emma Lathrop,^{1,2} Dea Musa,¹ Brent D. Newman,¹ Chonggang Xu,¹ Rachael E. McCaully,³ Carli A. Arendt,³ Verity G. Salmon,⁴ Amy Breen,⁵ Vladimir Romanovsky,⁶ Katrina E. Bennett,¹ Cathy J. Wilson,¹ and Stan D. Wulfschleger⁴

¹Earth and Environmental Sciences Division, Los Alamos National Laboratory, Bikini Atoll Road, Los Alamos, New Mexico, 87545, [USA](#)

²Center for Ecosystem Science and Society, Department of Biological Sciences, Northern Arizona University, Flagstaff, AZ, 86011, USA

³Department of Marine Earth and Atmospheric Sciences, North Carolina State University, Raleigh, North Carolina, 27695, [USA](#)

⁴Biological and Environmental Systems Science Division and Climate Change Science Institute, Oak Ridge National Laboratory, Oak Ridge, Tennessee, 37831, [USA](#)

⁵International Arctic Research Center, P.O. Box 757340, University of Alaska, Fairbanks, Alaska 99775-7340, USA

⁶Geophysical Institute, University of Alaska Fairbanks, Fairbanks, Alaska, 99775, [USA](#)

Correspondence to: Nathan Alec Conroy (nconroy@lanl.gov)

Abstract. Soil pore water (SPW) chemistry can vary substantially across multiple scales in Arctic permafrost landscapes. The magnitude of these variations and their relationship to scale are critical considerations for understanding current controls on geochemical cycling and for predicting future changes. These aspects are especially important for Arctic change modelling where accurate representation of sub-grid variability may be necessary to predict watershed scale behaviours. Our research goal was to characterize intra- and inter-watershed soil water geochemical variations at two contrasting locations in the Seward Peninsula of Alaska, USA. We then attempt to establish which environmental factors were important for controlling concentrations of important pore water solutes in these systems. The SPW geochemistry of 18 locations spanning two small Arctic catchments were examined for spatial variability and its dominant environmental controls. The primary environmental controls considered were vegetation, soil moisture/redox condition, water/soil interactions and hydrologic transport, and mineral solubility. The sampling locations varied in terms of vegetation type and canopy height, presence or absence of near-surface permafrost, soil moisture, and hillslope position. Vegetation was found to have a significant impact on SPW NO_3NO_2^- concentrations, associated with the localized presence of nitrogen-fixing alders and mineralization and nitrification of leaf litter from tall willow shrubs. The elevated NO_3NO_2^- concentrations were however, frequently equipoised by increased microbial denitrification in regions with sufficient moisture to support it. Vegetation also had an observable impact on soil moisture sensitive constituents, but the effect was less significant. The redox conditions in both catchments were generally limited by Fe reduction, seemingly well-buffered by a cache of amorphous Fe hydroxides, with the most reducing conditions found at sampling locations with the highest soil moisture content. Non-redox-sensitive cations were affected by a wide variety of water-soil interactions that affect mineral solubility and transport. Identification of the dominant controls on current SPW hydrogeochemistry allows for qualitative prediction of future geochemical trends in small Arctic catchments that are likely to experience warming and permafrost thaw. As source

Formatted: Subscript

Formatted: Subscript

39 areas for geochemical fluxes to the broader Arctic hydrologic system, geochemical processes occurring in these
40 environments are particularly important to understand and predict with regards to such environmental changes.

41 **1. Introduction**

42 Permafrost thaw in the Arctic is causing significant changes to landscape structure (Kokelj and Jorgenson, 2013;
43 Rowland et al., 2010), hydrology (Hiyama et al., 2021; Kurylyk et al., 2021; Liljedahl et al., 2016; Vonk, Tank, and
44 Walvoord, 2019; Walvoord and Kurylyk, 2016), vegetation (Lara ~~et al., Nitze, Grosse, and McGuire~~, 2018; Myers-
45 Smith et al., 2011; Sturm, Racine, and Tape, 2001; K. D. Tape ~~et al., Hallinger, Welker, and Ruess~~, 2012; ~~K-~~Tape,
46 Sturm, and Racine, 2006;), and biogeochemistry (O'Donnell et al., 2021; Frey and McClelland, 2009; Salmon et al.,
47 2019; Vonk, Tank, and Walvoord, 2019). The integrated hydrogeochemical effects of these environmental changes
48 are already apparent in the chemistry of the large Arctic rivers, where fluxes of carbon and nutrients are increasing,
49 leading to enhanced nutrient loadings, with strong implications for the global carbon cycle (Bring et al., 2016; Fuchs
50 et al., 2020; McClelland et al., 2016). While the watershed areas of large Arctic rivers are vast, recent studies suggest
51 that solute concentrations in these large rivers are likely controlled by solute generation processes occurring at much
52 smaller scales (Harms and Ludwig, 2016; Koch ~~et al., Runkel, Striegl, and McKnight~~, 2013; Shogren et al., 2019;
53 Vonk et al., 2015).

54 While there is a rapidly growing body of literature focused on observing and understanding environmental changes
55 over time with further Arctic warming, relatively few studies directly address the existing spatial variability, within
56 catchments or across catchments, and we are not aware of any studies that have combined field observations with
57 thermodynamic modelling in an effort to understand the causes of the existing spatial variability. Therefore, we have
58 a limited understanding of the key environmental controls on the spatial distribution of soil pore water solute
59 concentrations. In this study, we quantitatively evaluate the spatial variability of soil pore water (SPW) geochemistry
60 within and between two distinct catchments underlain with permafrost, and then seek to identify the source of the
61 observed spatial variability.

62 This study takes advantage of a scientifically diverse array of observations and datasets made available by the Next
63 Generation Ecosystem Experiment (NGEE) Arctic project, sponsored by the US Department of Energy Office of
64 Science. Most of the locations studied herein were selected by the NGEE Arctic project to provide co-located
65 measurements in a wide range of vegetation types, nested within representative hillslopes and catchments. Although
66 selected largely to represent a range of vegetation structure, such as shrub abundance and canopy height, these
67 locations also have considerable variability in other environmental parameters including, but not limited to: soil
68 moisture and temperature, presence or absence of near-surface permafrost, and maximum observed thaw depth (**Table**
69 **1** and **Table 2**). The vegetation-delineated sampling approach ~~presented here~~ provides an opportunity to not only
70 quantify the biogeochemical variability of SPW in Arctic environments, but also to investigate the root causes of that
71 observed variability. Data from additional sampling locations, available from a ~~collaborative-co-located~~ study, were
72 also utilized when possible.

73 Our overarching hypothesis is that vegetation-type and hillslope position are the dominant controls on spatial
74 variability of SPW geochemistry ~~at the NGEE Arctic field sites located on the Seward Peninsula~~. Vegetation-type

75 seems likely to have a significant effect on SPW geochemistry both directly and indirectly. Indirect effects would
76 include vegetation canopy impacts on soil moisture (through evapotranspiration and snow trapping). Direct effects of
77 vegetation would include nutrient cycle changes resulting from the annual deposition of plant litter. Such a direct
78 effect can be augmented at sites populated by alder shrubs due to this genus of deciduous shrubs ability to form a
79 symbiotic relationship with nitrogen-fixing *Frankia*, which they host in underground root nodules. Nitrogen fixation
80 associated with alders has previously been shown to accelerate local nitrogen cycling (Binkley et al., 1992; Clein and
81 Schimel, 1995; Bühlmann et al., 2014). Directly, through the increased cycling of some solutes (e.g. increased nitrogen
82 concentrations in the vicinity of alders, which add nitrogen to soils via a symbiotic relationship with nitrogen-fixing
83 bacterium; Salmon et al., 2019), and indirectly, through effects on soil moisture (i.e. evapotranspiration and trapping
84 of snow). Soil moisture will also affect SPW geochemistry, particularly of redox sensitive species, by limiting oxygen
85 diffusion and thus controlling which regions develop anoxic/reducing geochemical conditions. Soil moisture impacts
86 will likely be correlated with vegetation-type as well as hillslope position, and the presence or absence of perching
87 layers, including permafrost, all of which impact the vertical and horizontal drainage characteristics of a watershed.
88 Chemical species that are not redox-sensitive or controlled by biogeochemical reactions are likely to be
89 ~~effeted~~affected by transport, solubility, and water/sediment/organic matter interactions, and therefore largely
90 controlled by hillslope position as well as soil moisture.

91 Identifying the dominant controls on solute concentration variability within each catchment and across catchments
92 will facilitate better projections of future soil pore hydrogeochemistry in permafrost landscapes, and how these
93 signatures are related to changing soil moisture and increasing ~~in~~ tundra shrub abundance in a changing Arctic (Bring
94 et al., 2016; Myers-Smith et al., 2011; Prowse ~~et al.~~, Bring, Mård, and Carmack, 2015; Salmon et al., 2019; Sturm et
95 al., 2001; ~~K. D.~~ Tape et al., 2012; ~~K.~~ Tape et al., 2006; Wrona et al., 2016, 2016). Arctic warming and associated
96 permafrost thaw will increase hydrological connectedness between terrestrial and aquatic environments through
97 deepening of the active layer and the formation of deeper, more coherent groundwater flow paths (Bring et al., 2016;
98 Harms and Jones, 2012; Prowse, ~~Bring, Mård, Carmack,~~ et al., 2015a; Prowse, ~~Bring, Mård, and Carmack,~~ et al.,
99 2015b). Meanwhile, changes in hydrogeochemical signatures in larger Arctic rivers are likely to originate in smaller
100 catchments (McClelland et al., 2016; Prowse ~~et al.~~, ~~Bring, Mård, and Carmack,~~ 2015; Shogren et al., 2019; Spence,
101 ~~et al., Kokelj, McCluskie, and Hedstrom,~~ 2015). In this sense, changes in hydrogeochemistry in small Arctic
102 catchments not only impact hydrogeochemistry at much larger scales, but also prognosticate the future
103 hydrogeochemistry of larger Arctic rivers.

104 2. Methods

105 2.1 Site Descriptions

106 This study focuses on two sites with permafrost on the Seward Peninsula of western Alaska, the Teller-27 Catchment
107 and the Kougarak-64 Hillslope (**Figure 1**). The Teller-27 Catchment, henceforth “Teller,” is a small (~2.25 km²)
108 headwater catchment located west of mile marker 27 along the Nome-Teller Highway northwest of Nome, Alaska.
109 The Kougarak-64 Hillslope, henceforth “Kougarak,” is a hillslope (~2.0 km²) located west of mile marker 64 along

Formatted: Font: Italic

Formatted: Font: Not Italic

Formatted: Superscript

Formatted: Superscript

110 the Nome-Taylor Highway northeast of Nome, Alaska. We utilized data from “intensive stations” at both Teller and
111 Kougarak where concentrated, multi-year, co-located observations of soil water chemistry, vegetation characteristics,
112 soil moisture and temperature, and other measurements have been collected as part of the NGEE Arctic Research
113 Project. These are identified as TL# (Teller Station #) or KG# (Kougarak Station #) in **Figure 2** and **Figure 3**,
114 respectively. It should be noted that Teller and Kougarak are not “paired watersheds” in the classical sense, differing
115 in only one major characteristic, which provides the basis for comparison. Instead, Teller and Kougarak differ in many
116 respects and are both representative of the broad range of hillslope conditions common on the Seward Peninsula.
117 Detailed descriptions of Teller and Kougarak have been published previously (Jafarov et al., 2018; Léger et al., 2019;
118 Philben et al., 2019, 2020; Salmon et al., 2019; Yang et al., 2020), therefore, only the catchment characteristics that
119 are probable sources of variability in SPW chemistry will be highlighted here.

120 Teller is a discrete catchment with a well-defined central drainage, a vertical declivity of approximately 200 m, and a
121 catchment area of approximately 2.25 km². Temperature probes, soil pits, coring activities, and geophysical
122 interpretations at Teller have confirmed the catchment is underlain with discontinuous permafrost (Léger et al., 2019).
123 The upper shoulder of Teller (near Station 5, **Figure 2** and **Figure 5**) is underlain with near-surface permafrost and
124 appears to be a degraded peat plateau. The resultant microtopography of the degraded peat and the shallow perching
125 horizon caused by the permafrost creates a landscape of unsaturated peat mounds surrounded by ponds and saturated
126 soils. Downslope of the peat plateau, the Teller hillslope has highly variable soil moisture and vegetation (**Table 1**).
127 The microtopography within the lower footslope looks similar to the upper shoulder, but the peat appears more
128 severely degraded and the cause of the perched water table is less clear. Léger et al. (2019) suggest the presence of
129 permafrost at a depth of 1 – 2 m at Teller Station 9 (**Figure 2**), but the perching could also be caused by a layer of silt,
130 at a depth of approximately 30 cm (Graham et al., 2018). The full extent of permafrost and silt in this region of the
131 catchment remains unknown, but the thaw depth in July 2018 was greater than 1 m and maintained a perched water
132 table (Philben et al., 2020), suggesting perching could be the result of silt rather than permafrost. Vegetation type,
133 moisture content, permafrost extent, and hillslope position for all Teller Stations are summarized in **Table 1**.

134 Kougarak differs in many ways from Teller, although both have characteristics that are typical of hillslopes on the
135 Seward Peninsula. Kougarak is a convex hillslope, with a vertical declivity of approximately 70 meters. The study
136 area at Kougarak is approximately 2.0 km². Soil temperature measurements at Kougarak suggest that the vast majority
137 of the site is underlain by shallow continuous permafrost (Romanovsky, Cable, and Dolgikh, 2020a); Kougarak
138 Station 5 is an exception, where the permafrost is deeper (Romanovsky et al., 2020a). The upper shoulder of Kougarak
139 is a well-drained rocky outcrop composed of metagranitic rock (Hopkins et al., 1955; Till, Dumoulin, Werdon, and
140 Bleick, 2011). Saturated soils are not prevalent until the footslope and the lower backslope, where Kougarak Stations
141 2, 11, 10, 1, and 6 are situated (**Figure 3**). The lower backslope is characterized by persistent saturation between
142 ubiquitous tussocks, formed by the tussock cotton grass *Eriophorum vaginatum*. The tussock-lichen tundra at
143 Kougarak introduces microtopography and spatially variable saturation; in this sense, the Kougarak tussocks are
144 analogous to the peat mounds and hummocks at Teller, but on different spatial scales and formed by different
145 processes. Kougarak has numerous patches of alder shrubland in an altitudinal band within the upper backslope; it
146 should be emphasized that Teller lacks tussock-lichen tundra and alder (*Alnus viridis* ssp. *fruticosa*) shrubs that are a

Formatted: Superscript

Formatted: Superscript

147 feature of Kougarak. While continuous permafrost largely remains, the Kougarak site appears to be undergoing
148 environmental changes as evidenced by an increase in alder coverage over the past decades (Salmon et al., 2019). Soil
149 profiles underneath the alder patches are rocky with shallow bedrock and warmer permafrost (**Table 2**). Shrub tundra
150 (alder savanna in tussock tundra and willow-birch tundra) dominates the lower backslope, where the annual active
151 layer thickness is typically less than 100 cm. Vegetation type, moisture content, permafrost extent, and hillslope
152 position at all Kougarak stations are summarized in **Table 2**.

153 2.2 Sampling & Analytical Approach

154 SPWs were sampled using two complimentary techniques. Fiberglass wicks (Frisbee [et al.](#), [Phillips, Campbell, and](#)
155 [Hendriekx](#), 2010) were deployed in the upper 30 cm of soils at stations where shallow soils were unsaturated. These
156 wicks were left in place from year-to-year and only replaced if damage was observed or suspected. The sample
157 reservoirs from the wicks were collected whenever possible, usually a few times each summer. MacroRhizons
158 (Rhizosphere Research Products; Netherlands) were used at stations that were more saturated, also targeting the upper
159 30 cm of soils. Both techniques were used at stations of intermediate saturation, where both could be deployed
160 effectively. MacroRhizons represent a relatively discrete temporal sampling event (minutes to hours), whereas wicks
161 represent a cumulative water collected over longer periods (weeks to months). It is in this sense, that the two techniques
162 are complimentary. Unfortunately, due to saturation variability both techniques could not be used at all stations and
163 conditions at some Kougarak stations were sometimes too dry to collect meaningful volumes of SPW using either
164 method. Additional SPW data from Kougarak were supplemented from a separate study focused on alder-related
165 nutrient dynamics (McCaully et al., [2022In-Review](#)). These data were collected by MacroRhizons and are captured
166 as Kougarak Stations 10 – 13, which were not part of the original stations established by the NGEE Arctic Program.
167 A total of 309 SPW samples from Kougarak were collected and analysed, whereas a total of 89 SPW samples from
168 Teller were collected and analysed.

169 After collection, SPW cation concentrations were measured in triplicate by inductively coupled plasma optical
170 emission spectroscopy (Optima 2100 DV; PerkinElmer, USA) following US EPA Method 200.7. Inorganic anion
171 concentrations were measured by ion chromatography (DX-600; Dionex, USA) following US EPA Method 300.0. B,
172 F, K, Na, and Si concentrations collected by wicks were excluded from the dataset due to known issues with these
173 ions leeching from fiberglass wick samplers (Perdrial et al., 2014; Wallenberger and Bingham, 2009). This effect is
174 illustrated in [Supplementary Figure 1](#) and the lack of such an effect for divalent cations is shown in [Supplementary](#)
175 [Figure 2](#). Comparison of data from wicks and MacroRhizons, along with the observations from (Perdrial et al., 2014),
176 demonstrates that remaining constituents discussed herein were not affected by collection with fiberglass wicks.
177 Alkalinity, pH, and E_H are all critical geochemical parameters that are susceptible to change during storage (Petrone
178 [et al.](#), [Hinzman, Shibata, Jones, and Boone](#), 2007); because of the large amount of data from wicks these parameters
179 were not considered further, except in the context of thermodynamic modelling.

180 Observations related to vegetation, soil moisture, and permafrost extend were compiled from datasets made available
181 by the NGEE Arctic project and are given for Teller in **Table 1** and for Kougarak in **Table 2**. The reported soil
182 moisture contents were derived from an average of gravimetric measurements (2017 and 2018) and time domain

Formatted: Font: Bold

Formatted: Font: Bold

183 reflectometry measurements (2017 and 2019), and from remotely-sensed P-band Synthetic Aperture Radar (2017).
184 End-of-winter snow depths were measured in March and April of 2016, 2017, and 2018. The annual average ground
185 temperature was measured using in-situ temperature sensors (HOBO U30 DataLogger) at a depth of 1.5 meters below
186 the ground surface (Romanovsky et al., 2020a; Romanovsky, Cable, and Dolgikh, 2020b) and the active layer
187 thicknesses were determined by frost probe in September 2019 at the end of the growing season. Vegetation data were
188 collected at the peak of the growing season in mid to late July 2016 and 2017 at the NGEE Arctic Kougarok and Teller
189 field sites, respectively. The distribution of plant communities in the Arctic is primarily controlled by landscape,
190 topography, soil chemistry, soil moisture, and the plants that historically colonized an area (Raynolds et al., 2019).
191 Soil available rooting depth, which can be limited by shallow depths to bedrock, permafrost, or the water table, can
192 also restrict plant growth and survival of certain species by reducing access to water and nutrients. We surveyed the
193 dominant plant communities along each hillslope, which varied in their shrub abundance, canopy height, and structure,
194 to characterize the vegetation composition at the sites following the recommended protocol of Walker et al. (2016).
195 Extensive field site details and vegetation sampling methods are more thoroughly described in previous studies
196 (Salmon et al., 2019; Langford et al., 2019; Yang et al., 2020; Sulman et al., 2021; Yang et al. 2021).
197 For this study, we provide summary statistics for vegetation plots associated with intensive stations. Vegetation
198 composition plots within each intensive station were chosen subjectively in areas of homogeneous and representative
199 vegetation varying in size from 1 to 25 m² depending on canopy structure and height. The surveyed plot area was 1 ×
200 1 m for all plant communities except for the taller stature willow-birch tundra, mesic willow shrubland (2.5 × 2.5 m),
201 and alder shrubland (5 × 5 m). For each plot, all plant species (vascular plants, lichens, and bryophytes) were recorded
202 along with visual estimates of their percent cover. For plots with multiple canopies, field cover estimates were recorded
203 as absolute cover, meaning that the total cover per plot can be >100%. We calculated relative cover values (adding to
204 100%) from the field data and use these for all subsequent analyses.
205 Plant species were further aggregated into nine plant functional types (PFTs), groupings of plant species that share
206 similar growth forms and roles in ecosystem function (Wullschleger et al., 2014), based on growth patterns and plant
207 traits. PFTs in this study include: (1) nonvascular mosses and lichens, (2) deciduous and evergreen shrubs of various
208 height classes, including an alder PFT, (3) graminoids, and (4) forbs. Photos of representative PFTs from both sites
209 are given in **Supplementary Figures 9-17**. Canopy height was estimated within each plot for each PFT as the average
210 of 4 measurements, including a maximum canopy height. Active layer depth was measured at the end of the growing
211 season for all plots in September 2018 using a frost probe. A temperature probe was used to determine if the resistive
212 layer was permafrost (<0 °C) or rock (>2 °C). Thaw depth is an average of 4 measurements from the vegetation plot
213 corners.

Formatted: Superscript

Formatted: Font: Bold

214 2.3 Statistical Analysis

215 Principal Components Analysis (PCA) and the Mann-Whitney U-Test (MWUT) were both used to investigate
216 dominant environmental controls on solute concentrations in SPWs at Teller and Kougarok. PCA is an exploratory
217 data analysis tool that reduces the dimensionality of large complex datasets and considers how components (i.e. solute
218 concentrations) vary together. Because PCA was predominately used as a screening tool to reveal geochemical

219 correlations that may not have been evident by traditional geochemical causations or inference, a detailed discussion
220 of the PCA results is reserved to the Supplementary Materials. The MWUT was used to test for significant differences
221 in solute concentrations between Teller and Kougarok (inter-site variability) and between stations at each site (intra-
222 site variability). The MWUT is a non-parametric method of challenging a null hypothesis, which in this case is the
223 assumption that the concentrations of a given solute are not systematically greater at either site nor at any particular
224 station. Water chemistry data are typically not normally distributed and thus, non-parametric difference tests such as
225 the MWUT are preferred. The MWUT challenges the distribution of values, not the means. In this work, the level of
226 significance associated with the null hypothesis was operationally defined as 0.05, which equates to a 95 % chance
227 that an observed statistical difference is real and not coincidental. This error rate is operationally defined per contrast
228 (i.e. a 95 % chance that the observed statistical difference in nitrate concentrations between Teller Station 9 and Teller
229 Station 7 is real or that the observed statistical difference in sulphate concentrations between Teller and Kougarok is
230 real) as opposed to familywise (i.e. a 95 % chance that all of the observed/reported statistical differences are real and
231 not coincidental). MWUTs were completed using the methods described in Corder and Foreman (2009) and PCA was
232 completed using packages available in R statistical software, version 3.3.6 (Corder and Foreman, 2009; R Core Team,
233 2020). For all analyses, concentrations below the method detection limit were operationally defined as half the
234 detection limit, in agreeance with (Helsel, 2005, p. 43). While the emphasis of this study was on site/station (i.e.
235 spatial) variability, it should be recognized that seasonal and inter-annual variability could also be significant. To
236 minimize seasonal forcing on the variability observed, all SPW geochemical data presented were collected during the
237 thaw season between June and September.

238 **2.4 Thermodynamic Modelling**

239 To investigate thermodynamic controls on solute behaviour, particularly solubility limitations, thermodynamic
240 modelling exercises were undertaken using PHREEQC, a thermodynamic geochemical modelling code, and
241 PhreePlot, which facilitates repetitive PHREEQC calculations through looping (Kinniburgh and Cooper, 2011;
242 Parkhurst and Appelo, 2013). Because this study was focused on elucidating the primary geochemical controls on
243 solute concentrations in SPWs and not on developing a rigorous transport model, representative concentrations were
244 used instead of station specific concentrations. Representative “low”, “median”, and “high” concentration conditions
245 were proxied from the 25th, 50th, and 100th concentration percentiles, respectively, taken from both Teller and
246 Kougarok (Supplementary **Table 4**). Meanwhile, representative pH and E_H ranges were determined either through
247 direct measurement (pH), or indirectly by correlating dissolved Fe^{2+} concentrations and pH with a redox condition
248 through geochemical models and the Nernst equation. Modelling exercises were performed at 25 °C—utilizing the
249 phreeqc.dat database, with the only modification being the suppression of methane production by inorganic carbonate
250 reduction. Modelling exercises were performed at the default PHREEQC modelling temperature (25 °C), as the
251 selection of an alternative defensible temperature was non-trivial: temperatures on the Seward Peninsula span a very
252 wide range and its unclear what temperature would be most suitable for mineral solubility limitation modelling.
253 Ultimately, because the thermodynamic models were used as a tool understand what could be controlling soil pore
254 water solute concentrations and were not intended to model the system or to predict future concentrations, the default

255 temperature was decided to be the most suitable. While there is some temperature dependence of mineral solubility,
256 the differences in predicted solubility between 4 °C and 25 °C did not impact the interpretation of our results
257 (Supplementary Figure 8). Methane production was “turned-off” to maintain carbonate availability under reducing
258 conditions to help identify any possible carbonate minerals that could be precipitating. Because alkalinity was only
259 measured in a small number of samples, carbonate concentration percentiles were estimated from charge imbalances.
260 Alkalinity and charge imbalance were very well correlated in samples where alkalinity was measured
261 (Supplementary Figure 3). Although not a particularly rigorous modelling exercise, this approach was sufficient to
262 identify mineral phases that could be controlling solute generation processes through solubility limitations.

Formatted: Font: Bold

Formatted: Font: Bold

263 3. Results

264 3.1 Physical Characteristics of Stations (Co-Located Studies)

265 Controls on the observed spatial variability of SWP solute concentrations at Teller and Kougarok stations were
266 deduced, in part, from differences in physical features and conditions of each station. Quantitative measures of many
267 of these physical characteristics were available from the interdisciplinary studies co-located at the Teller and Kougarok
268 stations. The extent of permafrost, ground temperature, active layer depth, soil moisture content, snow depth,
269 vegetation type, vegetation canopy height, dominant plant functional type, and hillslope position were all compiled
270 from these co-located studies. Using these measures, the physical characteristics of each station are summarized in
271 Table 1 and Table 2, grouped by vegetation type.

272 3.1.2 Inter-site Variability: Teller versus Kougarok

273 Mann-Whitney U-Testing revealed that the concentrations of 14 of the 23 constituents analysed were significantly
274 different ($1.96 < |z|$) between Teller and Kougarok (Table 3). The effect size, a measure of how significantly different
275 the concentrations were, were large for Na and F; medium-large for K and Si; medium for Al, Oxalate, B, Zn, $\text{SO}_4\text{SO}_4^{2-}$
276 , Fe, Ba, Ti, and NO_3^- ; and small-medium for Li. The terminology and thresholds for these semi-quantitative
277 differences in correlation were taken from Corder and Foreman (2009). Mann-Whitney U-testing revealed that SPW
278 concentrations of many constituents were significantly different between Teller and Kougarok (Table 3). When
279 concentrations were significantly different between the sites, Kougarok generally exhibited the higher concentrations
280 of the two. SPW concentrations of Na, F, K, Si, Al, oxalate, B, Zn, Fe, Ba, Ti, NO_2 , and Li were all significantly
281 greater at Kougarok than Teller, while only SO_4^{2-} concentrations were significantly greater at Teller. Meanwhile, the
282 concentrations of Br, NO_3^- , Sr, PO_4 , Mg, Cr, Mn, Cl, and Ca were not significantly different between Teller and
283 Kougarok. When concentrations were significantly different between the sites, Kougarok generally exhibited the
284 higher concentrations of the two. Only SO_4 concentrations were significantly greater at Teller. The concentrations of
285 Br, NO_3 , Sr, PO_4 , Mg, Cr, Mn, Cl and Ca were not significantly different between Teller and Kougarok. A summary
286 of the inter-site MWUT results are given in Table 3 with the constituents that exhibited significant differences between
287 the sites displayed over a darkened background.

Formatted: Subscript

Formatted: Superscript

288 **3.23 Intra-site Variability: Teller and Kougarok Stations**

289 Mann-Whitney U-Testing was also used to test for intra-site differences between stations at both Teller and Kougarok.
290 Boxplots and compact letter displays are used to visualize the within-site variability of a select group of constituents
291 of interest (COIs), which are given in **Figure 4**. Tables of the results of the intra-site MWUTs for all constituents that
292 were monitored, including those that did not demonstrate some systematic inter-station variability or were not
293 otherwise of interest, are given in the Supplementary Materials.

294 **3.3 Physical Characteristics of Stations (Co-Located Studies)**

295 Controls on the observed spatial variability of SPW solute concentrations at Teller and Kougarok stations were
296 deduced, in part, from differences in physical features and conditions of each station. Quantitative measures of many
297 of these physical characteristics were available from the interdisciplinary studies co-located at the Teller and Kougarok
298 stations. The extent of permafrost, ground temperature, active layer depth, soil moisture content, snow depth,
299 vegetation type, vegetation canopy height, dominant plant functional type, and hillslope position were all compiled
300 from these co-located studies. Using these measures, the physical characteristics of each station are summarized in
301 **Table 1** and **Table 2**, grouped by vegetation type.

302 **4. Discussion**

303 **4.1 Inter-site Variability: Teller versus Kougarok**

304 Mann-Whitney U testing revealed that SPW concentrations of many constituents were significantly different between
305 Teller and Kougarok (**Table 3**). SPW concentrations of Na, F, K, Si, Al, oxalate, B, Zn, Fe, Ba, Ti, NO₂, and Li were
306 all significantly greater at Kougarok than Teller, while only SO₄ concentrations were significantly greater at Teller.
307 Meanwhile, the concentrations of Br, NO₃, Sr, PO₄, Mg, Cr, Mn, Cl, and Ca were not significantly different between
308 the two sites. Overall, the more frequent instance of significantly greater constituent concentrations at Kougarok
309 suggests a systematic cause. The extensive low gradient toeslope (**Figure 2**) and lack of a well defined drainage
310 channel at Kougarok, are likely causes of the systematically higher SPW solute concentrations at Kougarok. Water
311 perching, the result of near surface permafrost in the lower backslope and toeslope, increases evapotranspiration and,
312 thus, SPW solute concentrations. Meanwhile, the lack of a drainage channel at Kougarok suggests that runoff (and
313 therefore solute exports) is more limited than at Teller. Without a relatively rapid export mechanism such as a stream
314 channel, solute transport is likely limited to interflow within the Kougarok hillslope over much of the thaw season,
315 allowing weathering products to increase to significantly greater concentrations than those observed at Teller, where
316 a well defined drainage/export mechanism does exist. Field observations from pits at Kougarok confirm the present
317 of interflow at the site. The exception to the general observation of elevated concentrations at Kougarok versus Teller
318 was SO₄. Although the cause of consistently higher SO₄ concentrations at Teller is unclear from the limited scope of
319 this study, it seems likely to be due to a greater abundance of sulfidic bedrock material. The presence of sulfidic
320 bedrock in the vicinity of Teller has been reported by mineral prospecting efforts (Brobst, Pinckney, and Sainsbury,
321 1971; Herreid, 1966; Mulligan, 1965); we are unaware of any such reports near Kougarok.

4.2 Intra-site Variability: Teller and Kougarok Stations

Our interpretation of the major environmental controls on the observed spatial variability of SPW solute concentrations between stations are shown in Table 4. Each of these controls, including vegetation effects, soil moisture and redox effects, weathering, water/soil interactions and hydrological transport effects, and mineral solubility effects, is discussed-considered in detail in the following sections.

3.4.3.1 Vegetation Effects

Vegetation can influence hydrogeochemical variability directly via vegetation-induced changes to elemental cycling and soil moisture contents, or indirectly via the secondary impacts changes in soil moisture can have on mineral solubility or on the soil redox condition. The geochemical consequences of solubility and redox conditions are the focus of sections to follow, thus, this section will focus on direct vegetation effects via influences on elemental cycling and soil moisture via evapotranspiration and preferential trapping of snow.

NO_2NO_3^- was the only COI that showed a distinct effect from vegetation via elemental cycling.- Elevated NO_2NO_3^- concentrations were associated with the presence of alder shrubs and, in some cases, willow shrubs. NO_2NO_3^- concentrations at both sites were generally low, with the exception of Kougarok Stations 3, 5, and 12, and Teller Station 7 (Figure 4). **Low to tall alder shrubs are the dominant vegetation type at Kougarok Stations 3 and 12 (Table 2).** Meanwhile, alders are present at Kougarok Station 5 despite the dominant vegetation type being low willow and birch shrubs. Kougarok Stations 3, 5, and 12 all have a significant alder presence. Alders increase soil nitrogen through a symbiotic relationship with nitrogen-fixing bacteria that reside in their root nodules, thus, an association between NO_2NO_3^- concentrations and alder vegetation is expected (Salmon et al., 2019).

Perhaps more noteworthy was ~~the elevated NO_2 at Kougarok Station 5 and~~ the lack of elevated NO_2NO_3^- concentrations at Kougarok Stations 1, 2, 6, 10, and 11. The vegetation type at Kougarok Stations 1, 2, 6, 10, and 11 is alder savanna in tussock tundra, which is a mixed graminoid-shrub tundra with shorter stature and lower density of alder shrubs, yet nonetheless nitrogen input via alder derived nitrogen-fixation is anticipated to occur. The lack of elevated NO_2NO_3^- suggests either that 1) nitrogen-fixation in alder savanna in tussock tundra is insufficient to result in an increase in NO_2NO_3^- concentrations, 2) that the Kougarok footslope and lower backslope is very nitrogen-limited, and thus, that NO_2NO_3^- is largely consumed by vegetation as it is fixed, or 3) that microbes in the Kougarok footslope and lower backslope rapidly denitrify the available NO_2NO_3^- as a substitute for oxygen in their metabolisms. The smaller shrub size and density in the alder savanna in tussock tundra certainly results in less accumulated leaf litter relative to the denser and larger alder shrubland intensive stations, as such, it seems reasonable that less nitrogen would be available at stations in alder savanna in tussock tundra. Meanwhile, isotopic measurements of nitrogen downslope of alder patches at Kougarok Stations 12 and 3 also support the occurrence of denitrification (McCaully et al., In Review 2022). Therefore, we believe the lack of elevated NO_2NO_3^- concentrations at Kougarok Stations 1, 2, 6, 10, and 11 is a combination of less alder leaf litter and greater denitrification, than at Kougarok Stations 3, 5, or 12.

At Teller, only Station 7 exhibited elevated NO_2NO_3^- concentrations relative to the rest of the catchment (Figure 4). Teller Station 7 is dominated by tall willow shrubs and is relatively dry. Mineralization and nitrification of willow leaf litter coupled with limited microbial denitrification is the presumed cause of elevated NO_2NO_3^- concentrations at

Formatted: Heading 2,Sub_Heading

Formatted: Subscript

Formatted: Subscript

Formatted: Subscript

Formatted: Font: Bold

Formatted: Not Superscript/ Subscript

Formatted: Not Superscript/ Subscript

Formatted: Superscript

358 Teller Station 7. Teller Station 2 also has tall willow shrubs but did not exhibit elevated NO_3NO_3^- concentrations.
359 From the limited scope of this study, it is unclear why Teller Station 2 did not exhibit elevated NO_3NO_3^- while Station
360 7 did, but we suspect that higher seasonal moisture content and greater microbial denitrification at Teller Station 2
361 likely played a role. Also of note was that despite significant intra-site NO_3NO_3^- concentration differences, inter-site
362 differences were not significant ($|z| = 1.59$) and that relatively few Kougarak stations showed elevated NO_3NO_3^-
363 concentrations, despite a widespread alder presence. Increased microbial denitrification is suspected to balance
364 increased nitrogen-fixation at these stations. This is consistent with previous studies that have noted higher nitrogen
365 mineralization rates in acidic tundra than non-acidic tundra (Weiss et al., 2005); Kougarak is predominantly acidic
366 tundra and Teller is non-acidic tundra.

367 The effect of vegetation on spatial variability of soil moisture was not readily observed in the volumetric moisture
368 content of soil (Table 1 and Table 2) but was somewhat apparent in the spatial variability of moisture sensitive
369 constituents, such as Cl (Figure 4). The lack of a clear correlation between vegetation and soil moisture by TDR or
370 P-band SAR observations is perhaps due to the coarseness of the P-band SAR observations and the strong seasonality
371 associated with both methods. Moisture sensitive constituents, such as Cl, may provide a more seasonally averaged
372 tracer of soil moisture content at the stations. An increase in Cl concentrations with vegetation canopy height was
373 apparent at Teller stations suggesting an evapotranspiration effect. This trend was also apparent at Kougarak, but the
374 differences were rarely significant. Overall, the spatial variability of soil moisture sensitive constituents, like Cl, was
375 far less correlated with vegetation-type than expected; perhaps due to preferential trapping of snow, which may offset
376 the increased evapotranspiration of tall shrubs more than previously realized. Overall, Cl concentrations at Kougarak
377 appeared to be more correlated with hillslope position than with vegetation canopy height (Figure 4).

378 3.3.2.4.4 Soil Moisture and Redox Effects

379 Soil moisture content can have a profound effect on redox sensitive elements. Saturation limits oxygen diffusion into
380 soil, and thus, forces microorganisms to utilize less energetic electron acceptors to metabolize organic matter. In an
381 ideal system, soil microorganisms will use the strongest electron acceptor available, until it is exhausted. Although
382 natural environments are not ideal systems, redox conditions in soils follow a more or less stepwise progression.
383 Therefore, by evaluating the dissolved concentrations of NO_3NO_3^- , Mn, Fe, and $\text{SO}_4\text{SO}_4^{2-}$ in SPWs, it is possible to
384 qualitatively assess soil redox conditions and their impact on hydrogeochemical variability.

385 The redox conditions at both Teller and Kougarak are generally limited by Fe reduction, with the most reducing
386 conditions found at stations with the highest soil moisture content. As such, NO_3NO_3^- concentrations are generally
387 low (Table 3), $\text{SO}_4\text{SO}_4^{2-}$ concentrations are relatively consistent (Figure 4), and Mn and Fe concentrations increase
388 with increasing soil moisture (Figure 4). NO_3NO_3^- concentrations were generally low, except for drier stations in the
389 proximity of tall alders or willows. While NO_3NO_3^- inputs are discussed in the vegetation effects section, the lack of
390 high NO_3NO_3^- concentrations at wetter stations that contain alders suggests that soil moisture coupled with microbial
391 denitrification bears a strong control on SPW NO_3NO_3^- concentrations. Meanwhile, $\text{SO}_4\text{SO}_4^{2-}$ concentrations at both
392 sites are relatively constant across clear moisture and redox gradients (Figure 4). This suggests that $\text{SO}_4\text{SO}_4^{2-}$
393 reduction is not pervasive at either site. Dissolved Fe concentrations were higher at stations with higher soil moisture

Formatted: Not Superscript/ Subscript

Formatted: Superscript

394 content, consistent with Fe reduction. Similarly, Mn concentrations were slightly elevated at wetter stations. The
395 concentrations of Mn, however, rarely rose above 0.05 mg·L⁻¹, suggesting either Mn solubility limitations or a lack
396 of a significant Mn weathering source. Low Mn concentrations at Teller Station 5, a wetter station on the upper
397 shoulder of the Teller watershed (**Table 1; Figure 2**) seems to support the latter conclusion, as do geochemical
398 modelling exercises (Section 4.5). Together, these results suggest that the most reducing condition at both sites is
399 typically limited to Fe reduction and that this only occurs at stations with the highest soil moisture contents.

400 **4.43.3.3 Weathering, Water/Soil Interaction, and Hydrological Transport Effects**

401 A combination of weathering, water/soil interactions, and hydrological transport were ~~clear-identified as probable~~
402 drivers of hydrogeochemical variability for some solutes. As noted by Philben et al. (2020), soil derived solutes tend
403 to accumulate in low-lying areas within watersheds. This is ~~clearly-seenobserved~~ at Teller, where the concentrations
404 of Ca, Sr, and Mg all increase dramatically at the transition from lower backslope to footslope (**Figure 5**). Both Teller
405 and Kougarok are underlain by carbonate-rich metamorphic facies, and Ca, Sr, and Mg are probable carbonate counter-
406 cations. Weathering of Ca, Sr, and Mg carbonates and subsequent transport of these cations downslope explains this
407 pattern of spatial variability. At Kougarok, concentrations of Ca, Mg, and Sr similarly increase from upper backslope
408 to footslope, but concentrations of Ca and Sr decrease further down the lower backslope (Stations 10 and 1), while
409 Mg concentrations continue to increase. A possible explanation for this behaviour is the greater affinity of cation
410 exchange surfaces for Ca and Sr compared to Mg, thus, Ca and Sr are preferentially retained in the footslope whilst
411 Mg is transported further down the lower backslope (Sparks, 2003, p. 189).

412 **4.53.3.4 Mineral Solubility Effects**

413 Although redox reactions are rarely at equilibrium in natural environments, comparison of field data with equilibrium
414 models provides valuable semi-quantitative insight into the redox condition of natural environments. Because Fe
415 appeared to be limiting the development of more reducing conditions (Section 4.3), select samples from both sites
416 were measured for soluble Fe²⁺ following methods presented in Viollier et al. (2000). These concentrations of aqueous
417 Fe²⁺ were then compared with model-predicted concentrations of Fe²⁺, when coupled with an infinite Fe(OH)_{3(am)}
418 phase, across a range of pH values (2 – 10) and fixed E_H values of 400 mV, 200 mV, 0 mV, and -200 mV; activity
419 coefficients were assumed to be equal to 1. The measured and modelled Fe²⁺ concentrations are compared in **Figure**
420 **6**, where concentrations that were below the method detection limit (0.05 mg·L⁻¹) are set equal to 0.025 mg·L⁻¹ (half
421 the detection limit). Comparison of model predicted Fe²⁺ concentrations with field data suggests that while Teller
422 exhibits a narrower range of pH conditions than Kougarok, it exhibits a broader range of redox conditions (**Figure 6**).
423 Although several Fe²⁺ measurements were below the detection limit, suggesting oxidizing conditions, high Fe²⁺
424 concentrations in some samples suggested E_H values below 0 mV. Therefore, Fe redox conditions at Teller ranged
425 from mildly reducing to oxic and Fe redox conditions at Kougarok ranged from mildly oxic to oxic. Oxidation-
426 reduction potentials (ORPs), calculated from pH, Fe²⁺ concentrations, and the Nernst equation suggest that ORPs at
427 Teller were as low as -69 mV, while the lowest ORP at Kougarok was +134 mV (**Figure 6**). Maximum ORP values
428 could not be determined quantitatively as some Fe²⁺ concentrations were below Fe²⁺ detection limits, at both sites.

429 E_H/pH predominance diagrams were created from the 25th, 50th, and 100th concentration percentiles and are shown
430 in **Figure 7** for the COIs where precipitation of mineral phases were predicted under some conditions. The
431 concentrations for these diagrams were taken from filtered aqueous concentration data, thus, predicted mineral
432 precipitation is an indication of nearly saturated or over-saturated conditions. The range of E_H and pH conditions
433 observed at Teller and Kougarok are overlaid as solid yellow and solid blue lines, respectively. Only the predominance
434 diagrams that indicated possible mineral formation under the E_H/pH conditions present at either site are shown in
435 **Figure 7**. These phases included Fe(OH)_{3(am)} (Fe), siderite (Fe), Al(OH)_{3(am)} (Al), chalcedony (Si), barite (Ba and
436 SO₄), calcite (Ca), dolomite (Ca and Mg), and rhodochrosite (Mn). Predominance diagrams for the remaining key
437 COIs that were not predicted to form any mineral phases under any site conditions are given in **Supplementary Figure**
438 **4**.

439 -To further examine which mineral phases could be controlling ~~solute generation processes~~ **SPW solute concentrations**,
440 saturated conditions for the mineral phases identified in **Figure 7** were modelled using sweeps of pH values from 2 –
441 10 at various fixed E_H values (400mV, 200mV, 0mV, and -200mV). Predicted solute concentrations under the
442 modelled saturated conditions were then compared with field data to find common trends. In general, if solute
443 concentrations were frequently measured near the saturation of a mineral, or were identified to have similar
444 dependence on pH or E_H, it was inferred that the mineral phase could be controlling the generation of that solute. The
445 mineral phases that were identified to possibly be controlling solute concentrations were Al(OH)_{3(am)}, Fe(OH)_{3(am)},
446 chalcedony, and barite. This does not preclude the presence of significant concentrations of other mineral phases, it
447 only identifies these as ~~likely possibly~~ controlling the dissolved concentrations of Al, Fe, Si, and Ba, respectively.
448 Although it does not provide mineralogical information, X-ray fluorescence (XRF) data reported by another study at
449 Teller confirmed high concentrations of Al, Fe, Si, and Ba in the organic and mineral soil layers at that site (Graham
450 et al., 2018). We are unaware of any similar studies at Kougarok, nor are we aware of any studies that provide would
451 provide confirmatory mineralogical information, for example by X-ray diffraction (XRD).

452 Aluminium concentrations in SPWs at both Teller and Kougarok appear to be controlled by the
453 dissolution/precipitation of amorphous Al hydroxide (Al(OH)_{3(am)}) (**Figure 8**). The solubility limit of Al(OH)_{3(am)} has
454 no redox dependence, but is highly pH dependent. Aluminium concentrations were generally clustered near the
455 solubility limit of Al(OH)_{3(am)}; Al(OH)_{3(am)} + 3H⁺ ↔ Al³⁺ + 3H₂O; log k = 10.8. This suggests that Al SPW
456 concentrations at both sites are controlled by wetting/drying (dissolution/precipitation) processes. It also suggests that
457 there could be a significant amount of Al(OH)_{3(am)} in the soils at both sites. While organic matter may also sorb to
458 alumina surfaces, the adherence to the solubility of Al(OH)_{3(am)} suggests that significant concentrations of Al are not
459 complexed with dissolved organic matter. The predominance diagrams highlight 1) the strong pH dependence on the
460 stability of Al(OH)_{3(am)}, 2) the influence of dissolved F can have on Al speciation when Al concentrations are low,
461 and 3) that Al is a cation at low pH and an anion at high pH (**Figure 7**). Despite being a weathering product, Al
462 concentrations show a dissimilar downslope trend to other weathering products, especially at Teller (**Supplementary**
463 **Figure 5**). While the concentrations of weathering products generally increase with distance downslope, Al
464 concentrations decrease. We suspect this can be attributed to increasing pH with distance downslope. Philben et al.
465 (2020) reported a 1 pH unit increase in pH in organic soils along the Teller transect (**Figure 2**), increasing from 5.6 at

Formatted: Font: Bold

Formatted: Font: Bold

466 Station 5 to 6.7 at Station 9. Such an increase would decrease the solubility of $\text{Al}(\text{OH})_{3(\text{am})}$, and thus, decrease the
467 concentration of dissolved Al (**Figure 8**).

468 Similar to Al, Fe concentrations in SPWs at both Teller and Kougark appear to be controlled by the
469 dissolution/precipitation of amorphous Fe hydroxide ($\text{Fe}(\text{OH})_{3(\text{am})}$). Fe concentrations were generally clustered near
470 the solubility limit of $\text{Fe}(\text{OH})_{3(\text{am})}$ (**Figure 8**). Unlike $\text{Al}(\text{OH})_{3(\text{am})}$ however, $\text{Fe}(\text{OH})_{3(\text{am})}$ solubility is dependent on the
471 redox condition in addition to the pH; $\text{Fe}(\text{OH})_{3(\text{am})} + 3\text{H}^+ + \text{e}^- \leftrightarrow \text{Fe}^{2+} + 3\text{H}_2\text{O}$; $\log k = 16.0$ (**Figure 8**). Fe(III) is only
472 sparingly soluble in aqueous solutions and reduction to Fe(II) significantly increases the solubility of Fe, thus, at a
473 given pH value higher aqueous concentrations are predicted and observed under more reducing conditions (**Figure 8**).
474 Iron concentrations in SPWs at both sites generally follow the pH dependence of $\text{Fe}(\text{OH})_{3(\text{am})}$ solubility (**Figure 8**).
475 This suggests that SPW concentrations of Fe at both sites are controlled by wetting/drying (dissolution/precipitation)
476 processes, coupled with the redox condition.

477 Si concentrations are frequently limited by the solubility of chalcedony, a very finely grained form of SiO_2 , which is
478 much more soluble than quartz; $\text{SiO}_2 + 2\text{H}_2\text{O} \leftrightarrow \text{H}_4\text{SiO}_4$; $\log k = -3.55$. Particularly at Kougark, the dissolved Si
479 concentrations, coupled with a lack of a strong pH or E_{H} dependence, suggest a controlling influence of chalcedony.

480 Ba concentrations also appear to be controlled by solubility, but rather than by the solubility of an oxide or a hydroxide
481 phase, by the solubility of barite [$\text{Ba}^{2+} + \text{SO}_4^{2-} \leftrightarrow \text{BaSO}_4(\text{s})$; $\log k = 9.97$]. Unlike Al hydroxide or Fe hydroxide, barite
482 solubility lacks a strong pH dependence and instead is dependent solely on the activities of Ba^{2+} and SO_4^{2-} . Unlike Ba,
483 $\text{SO}_4\text{SO}_3^{2-}$ concentrations are not limited by the solubility limit of barite and are generally higher and not well correlated
484 with Ba concentrations. Together, these suggest that $\text{SO}_4\text{SO}_3^{2-}$ from another source (likely, atmospheric deposition or
485 sulfidic mineral oxidation), is suppressing barite dissolution, and thus, is reducing dissolved Ba concentrations. Barite
486 solubility can exhibit a redox dependence if conditions are sufficiently reducing to reduce $\text{SO}_4\text{SO}_3^{2-}$ to sulphide. This
487 shifts the equilibrium to greater dissolution of barite, and therefore higher conditions of Ba. The lack of E_{H} dependence
488 in observational data further suggests that neither site exhibits significant $\text{SO}_4\text{SO}_3^{2-}$ reduction.

489 **5.4. Conclusions Discussion**

490 The 18 stations examined herein (8 at Teller and 10 at Kougark) represent a wide range of vegetation types, soil
491 moisture contents, permafrost extents, and hillslope positions. Coupling the spatial variability of these landscape
492 characteristics with the spatial variability of SPW solute concentrations provides valuable insight into the dominant
493 environmental controls on observed spatial variability of SPW geochemistry. It is our hope that correlating SPW
494 geochemistry with readily observable and scalable landscape features will inform earth system modelling efforts in
495 permafrost regions and provide fast and easy methods to determine if earth system models are working properly (i.e.
496 predicting the correct trends). The inferred dominant environmental controls on the observed inter-site and intra-site
497 variability of SPW solute concentrations are discussed in the following sections.

Formatted: Subscript

498 **4.1 The Dominant Environmental Controls on Inter-site Variability of SPW Solute Concentrations**

499 Overall, the more frequent instance of significantly greater constituent concentrations at Kougarok suggests a
500 systematic cause. The extensive low-gradient toeslope (Figure 2) and lack of a well-defined drainage channel at
501 Kougarok, are likely causes of the systematically higher SPW solute concentrations at Kougarok. Water perching, the
502 result of near-surface permafrost in the lower-backslope and toeslope, increases evapotranspiration and, thus, SPW
503 solute concentrations. Meanwhile, the lack of a drainage channel at Kougarok suggests that runoff (and therefore
504 solute exports) is more limited than at Teller. Without a relatively rapid export mechanism such as a stream channel,
505 solute transport is likely limited to interflow within the Kougarok hillslope over much of the thaw season, allowing
506 weathering products to increase to significantly greater concentrations than those observed at Teller, where a well-
507 defined drainage/export mechanism does exist. Field observations from pits at Kougarok confirm observable interflow
508 at the site. Overall, our study suggests that evaporative concentration could be a significant control on SPW solute
509 concentrations in permafrost catchments, especially in those with limited drainage and therefore a perched near-
510 surface water table. This effect has been reported previously (Raudina et al., 2017), but does not appear to be widely
511 considered, perhaps due to the generally few studies of SPW solutes in permafrost regions. We suggest future efforts
512 to predict future SPW solute and nutrient dynamics directly address the impacts of evaporative concentration on
513 permafrost catchments, especially with future permafrost thaw.

514 The exception to the general observation of elevated concentrations at Kougarok versus Teller was SO_4^{2-} . Although
515 the cause of consistently higher SO_4^{2-} concentrations at Teller is unclear from the limited scope of this study, it seems
516 likely to be due to a greater abundance of sulfidic bedrock material. The presence of sulfidic bedrock in the vicinity
517 of Teller has been reported by mineral prospecting efforts (Brobst, Pinckney, and Sainsbury, 1971; Herreid, 1966;
518 Mulligan, 1965); we are unaware of any such reports near Kougarok.

Formatted: Normal

520 **4.5.12 The Dominant Environmental Controls on Intra-site Spatial Variability of SPW Solute Concentrations**

521 The 18 stations examined herein (8 at Teller and 10 at Kougarok) were selected to represent a wide range of vegetation
522 types, soil moisture contents, permafrost extents, and hillslope positions. Coupling the spatial variability of these
523 landscape characteristics with the spatial variability of SPW solute concentrations provides valuable insight into the
524 dominant environmental controls on observed spatial variability of SPW geochemistry.

525 With regard to our initial hypotheses, our major findings are that:

526 Vegetation influences on elemental cycles were only readily apparent for nitrogen and although vegetation induced
527 changes to soil moisture content were discernible, they were far less significant than anticipated. NO_3NO_2^- was the
528 only COI that exhibited a clear vegetation effect; elevated concentrations were associated with the presence of alder
529 shrubs and, in some cases, tall willow shrubs. These increases in NO_3NO_2^- concentrations associated with alder
530 nitrogen-fixation and the mineralization and nitrification of willow leaf litter were frequently equipoised by increased
531 microbial denitrification in regions sufficiently moist to support it, this is perhaps one of the most significant finding
532 of this work. Although both Kougarok and Teller exhibited some indications of increased Cl concentrations in the

Formatted: Subscript

Formatted: Subscript

533 presence of tall shrubs, the net vegetation effect on soil moisture was far less than hypothesized. Redox sensitivity
534 was also less than hypothesized and most stations seemed well-buffered at Fe redox conditions. The result of this
535 buffering was generally low NO_3NO_2^- concentrations (except where vegetation effects dominated), consistent
536 $\text{SO}_4\text{SO}_4^{2-}$ concentrations across clear redox gradients, and variable Mn and Fe concentrations. Mn concentrations were
537 generally low, likely due to a limited source. Fe concentrations were higher at stations with higher soil moisture
538 content, consistent with Fe reduction. Similar Fe redox cycling between soluble Fe(II) species and precipitated Fe
539 oxyhydroxides in permafrost catchments has been reported recently (Patzner et al., 2022), which suggests that Fe
540 redox buffering in permafrost landscapes is widespread. Weathering, water/soil interactions, and hydrological
541 transport were ~~clear~~-probable drivers of variability for Ca, Sr, and Mg. Ca, Sr, and Mg all tended to accumulate in
542 low-lying areas, although Ca and Sr demonstrated greater accumulation potential than Mg, likely via greater affinity
543 of cation exchange surfaces for Ca and Sr compared to Mg. Mineral solubility limitations were the primary controls
544 on Al ($\text{Al}(\text{OH})_{3(\text{am})}$), Fe ($\text{Fe}(\text{OH})_{3(\text{am})}$), Ba (barite), and Si (chalcedony) concentrations. This suggests that the SPW
545 concentrations of these constituents will remain stable until those mineral phases are exhausted or soil pore
546 hydrochemistry changes sufficiently to alter the solubility of those mineral phases. Supersaturation of Al with respect
547 to gibbsite (crystalline $\text{Al}(\text{OH})_3$) and Si with respect to chalcedony in a permafrost wetland has been reported
548 previously (Jesson et al., 2014). The solubility curves for gibbsite and $\text{Al}(\text{OH})_{3(\text{am})}$ are similar, with $\text{Al}(\text{OH})_{3(\text{am})}$ being
549 slightly more soluble at all pH values due to the increased thermodynamic stability of the crystalline Al hydroxide
550 mineral, gibbsite. Meanwhile, seasonal precipitation of Fe oxyhydroxides in permafrost peatlands and their effect of
551 carbon cycling was the subject of an excellent paper by Patzner et al. (2022). Our study is the first observation we are
552 aware of the saturation controls of barite on Ba in permafrost SPWs, although that could be because few relatively
553 few studies consider barium concentrations; it is worthwhile noting the Ba was not supersaturated with respect to
554 barite but approached a saturated condition. Future studies should also note that Cchanges in redox condition would
555 significantly alter $\text{Fe}(\text{OH})_{3(\text{am})}$ solubility, whereas changes in pH conditions would significantly alter $\text{Al}(\text{OH})_{3(\text{am})}$ and
556 $\text{Fe}(\text{OH})_{3(\text{am})}$ solubility.

557 Although discerning the environmental controls on spatial variability of SPW solute concentrations provides some
558 high-level insight into the effects changes in landscape character may have on soil pore hydrochemistry, our scope
559 was limited and leveraged on previously available datasets. The significance of SPW in small Arctic headwater
560 catchments as a key initial component in the freshwater hydrologic continuum is under recognized, and such
561 catchments warrant more detailed and systematic investigations.

Formatted: Subscript

Formatted: Subscript

563 **56. Acknowledgements**

564 We would like to thank the Sitnasuak Native Corporation and the Mary's Igloo Native Corporation for their guidance
565 and for allowing us to conduct this research on the traditional homelands of the Inupiat people. Funding was provided
566 by the Next-Generation Ecosystem Experiments (NGEE Arctic) project, supported by the Office of Biological and
567 Environmental Research in the U.S. DOE Office of Science. We wish to thank Lauren Charsley-Groffman and Nathan

568 Wales for their assistance with fieldwork, as well as, George Perkins, Oana Marina, Rose Harris, and Emily Kluk for
569 their assistance with laboratory analyses.

570 **76. Data availability statement**

571 The data that support the findings of this study are made openly available in the NGEE-Arctic data repository at (DOI:
572 10.5440/1735757).

573 **87. References**

574 [Anderson, M. D., Ruess, R. W., Myrold, D. D., and Taylor, D. L. \(2009\). Host species and habitat affect nodulation
575 by specific Frankia genotypes in two species of Alnus in interior Alaska. *Oecologia* 160, 619–630. doi:
576 10.1007/s00442-009-1330-0](#)

577 [Anderson, M. D., Ruess, R. W., Uliassi, D. D., and Mitchell, J. S. \(2004\). Estimating N₂ fixation in two species of
578 Alnus in interior Alaska using acetylene reduction and 15N₂ uptake. *Ecoscience* 11, 102–112. doi: 10.1080/
579 11956860.2004.11682814](#)

580 [Binkley, D., Sollins, P., Bell, R., Sachs, D., and Myrold, D.: Biogeochemistry of adjacent conifer and alder-conifer
581 stands, *Ecology*, 73, 2022–2033, 1992.](#)

582 Breen, A., Iversen, C., Salmon, V., VanderStel, H., Busey, B., and Wulschleger, S. 2020a.: NGEE Arctic Plant Traits:
583 Plant Community Composition, Kougarak Road Mile Marker 64, Seward Peninsula, Alaska, 2016 [Data set], doi:
584 <https://doi.org/10.5440/1465967>.

585 Breen, A., Iversen, C., Salmon, V., VanderStel, H., Busey, B., and Wulschleger, S. 2020b.: NGEE Arctic Plant Traits:
586 Plant Community Composition, Kougarak Road Mile Marker 64, Seward Peninsula, Alaska, 2016 [Data set], doi:
587 <https://doi.org/10.5440/1465967>.

588 Bring, A., Fedorova, I., Dibike, Y., Hinzman, L., Mård, J., Memild, S. H., ... Woo, M.-K. 2016: Arctic terrestrial
589 hydrology: A synthesis of processes, regional effects, and research challenges. *Journal of Geophysical Research:*
590 *Biogeosciences*, 121: 621–649, doi: <https://doi.org/10.1002/2015JG003131>.

591 Brobst, D. A., Pinckney, D. M., and Sainsbury, C. L. 1971: Geology and Geochemistry of the Sinuk River Barite
592 Deposit, Seward Peninsula, Alaska (No. 463 (?)). United States Department of the Interior Geological Survey.

593 [Bühlmann, T., Hiltbrunner, E., and Körner, C.: Alnus viridis expansion contributes to excess reactive nitrogen release,
594 reduces biodiversity and constrains forest succession in the Alps, *Alpine Botany*, 124, 187–191,
595 <https://doi.org/10.1007/s00035-014-0134-y>, 2014.](#)

596 [Clein, J. S. and Schimel, J. P.: Nitrogen turnover and availability during succession from alder to poplar in Alaskan
597 taiga forests, *Soil Biology and Biochemistry*, 27, 743–752, \[https://doi.org/10.1016/0038-0717\\(94\\)00232-P\]\(https://doi.org/10.1016/0038-0717\(94\)00232-P\), 1995.](#)

598 Conroy, N., Heikoop, J., Newman, B., Wilson, C., Arendt, C., Perkins, G., and Wulschleger, S. 2021: Soil Water
599 Chemistry and Water and Nitrogen Isotopes, Teller Road Site and Kougarak Hillslope, Seward Peninsula, Alaska,
600 2016 - 2019 [Data set], doi: <https://doi.org/10.5440/1735757>.

601 Corder, G. W., and Foreman, D. I. 2009: Nonparametric statistics for non-statisticians: a step-by-step approach.
602 Hoboken, N.J.; Wiley, 247 pp.

603 Frey, K. E., and McClelland, J. W. 2009: Impacts of permafrost degradation on arctic river biogeochemistry.
604 Hydrological Processes, 23: 169–182, doi: <https://doi.org/10.1002/hyp.7196>.

605 Frisbee, M. D., Phillips, F. M., Campbell, A. R., and Hendrickx, J. M. H. 2010: Modified passive capillary samplers
606 for collecting samples of snowmelt infiltration for stable isotope analysis in remote, seasonally inaccessible
607 watersheds 1: laboratory evaluation. Hydrological Processes, 24: 825–833, doi: <https://doi.org/10.1002/hyp.7523>.

608 Fuchs, M., Nitze, I., Strauss, J., Günther, F., Wetterich, S., Kizyakov, A., ... Grosse, G. 2020: Rapid Fluvio-Thermal
609 Erosion of a Yedoma Permafrost Cliff in the Lena River Delta. Frontiers in Earth Science, 8: 336, doi:
610 <https://doi.org/10.3389/feart.2020.00336>.

611 Graham, D. E., Kholodov, A., Wilson, C. J., Moon, J.-W., Romanovsky, V. E., and Busey, B. 2018: Soil Physical,
612 Chemical, and Thermal Characterization, Teller Road Site, Seward Peninsula, Alaska, 2016., doi:
613 <https://doi.org/10.5440/1342956>.

614 Harms, T. K., and Jones, J. B. 2012: Thaw depth determines reaction and transport of inorganic nitrogen in valley
615 bottom permafrost soils. Global Change Biology, 18: 2958–2968, doi: <https://doi.org/10.1111/j.1365->
616 [2486.2012.02731.x](https://doi.org/10.1111/j.1365-2486.2012.02731.x).

617 Harms, T. K., and Ludwig, S. M. 2016: Retention and removal of nitrogen and phosphorus in saturated soils of arctic
618 hillslopes. Biogeochemistry, 127: 291–304, doi: <https://doi.org/10.1007/s10533-016-0181-0>.

619 Helsel, D. R. 2005: Nondetects and data analysis: statistics for censored environmental data. Hoboken, NJ; Wiley-
620 Interscience, 250 pp.

621 Herreid, G. 1966: Preliminary geology and geochemistry of the Sinuk River area. Seward Peninsula, Alaska: Alaska
622 Division of Mines and Minerals Geologic Report, 24: 19.

623 Hiyama, T., Yang, D. and Kane, D.L., 2021. Permafrost Hydrology: Linkages and Feedbacks. In Arctic Hydrology,
624 Permafrost and Ecosystems (pp. 471-491). Springer, Cham.

625 [Hollingsworth, T. N., Lloyd, A. H., Nosssov, D. R., Ruess, R. W., Charlton, B. A., and Kielland, K. \(2010\). Twenty-](#)
626 [five years of vegetation change along a putative successional chronosequence on the Tanana River, Alaska. *Can. J.*](#)
627 [For. Res. 40, 1273–1287. doi: 10.1139/X10-094](#)

628 Hopkins, D. M., Karlstrom, T. N. V., Black, R. F., Williams, J. R., Pewe, T. L., Fernald, A. T., and Muller, E. H.
629 1955: Permafrost and ground water in Alaska. U.S. Geological Survey Professional Paper 264-F.

630 Jafarov, E. E., Coon, E. T., Harp, D. R., Wilson, C. J., Painter, S. L., Atchley, A. L., and Romanovsky, V. E. 2018:
631 Modelling the role of preferential snow accumulation in through talik development and hillslope groundwater flow in
632 a transitional permafrost landscape. Environmental Research Letters, 13: 105006, doi: <https://doi.org/10.1088/1748->
633 [9326/aadd30](https://doi.org/10.1088/1748-9326/aadd30).

634 [Jessen, Søren, Hanne D. Holmslykke, Kristine Rasmussen, Niels Richardt, and Peter E. Holm. 2014. "Hydrology and](#)
635 [Pore Water Chemistry in a Permafrost Wetland, Ilulissat, Greenland." *Water Resources Research* 50 \(6\): 4760–74.](#)
636 <https://doi.org/10.1002/2013WR014376>.

637 Kinniburgh, D., and Cooper, D. 2011: PhreePlot: Creating Graphical Output with Phreeqc.

638 Koch, J. C., Runkel, R. L., Striegl, R., and McKnight, D. M. 2013: Hydrologic controls on the transport and cycling
639 of carbon and nitrogen in a boreal catchment underlain by continuous permafrost. *Journal of Geophysical Research:*
640 *Biogeosciences*, 118: 698–712, doi: <https://doi.org/10.1002/jgrg.20058>.

641 Kokelj, S. V., and Jorgenson, M. T. 2013: Advances in Thermokarst Research. *Permafrost and Periglacial Processes*,
642 24: 108–119, doi: <https://doi.org/10.1002/ppp.1779>.

643 Kurylyk and Walvoord, 2021 Kurylyk, B.L. and Walvoord, M.A., 2021. Permafrost Hydrogeology. In *Arctic*
644 *Hydrology, Permafrost and Ecosystems* (pp. 493-523). Springer, Cham.

645 [Langford, Z. L., Kumar, J., Hoffman, F. M., Breen, A. L., & Iversen, C. M. \(2019\). Arctic vegetation mapping using](#)
646 [unsupervised training datasets and convolutional neural networks. *Remote Sensing*, 11\(1\), 1–23.](#)
647 <https://doi.org/10.3390/rs11010069>

648 Lara, M. J., Nitze, I., Grosse, G., and McGuire, A. D. 2018: Tundra landform and vegetation productivity trend maps
649 for the Arctic Coastal Plain of northern Alaska. *Scientific Data*, 5: 1–10, doi: <https://doi.org/10.1038/sdata.2018.58>.

650 Léger, E., Dafflon, B., Robert, Y., Ulrich, C., Peterson, J. E., Biraud, S. C., ... Hubbard, S. S. 2019: A distributed
651 temperature profiling method for assessing spatial variability in ground temperatures in a discontinuous permafrost
652 region of Alaska. *The Cryosphere*, 13: 2853–2867, doi: <https://doi.org/10.5194/tc-13-2853-2019>.

653 Liljedahl, A. K., Boike, J., Daanen, R. P., Fedorov, A. N., Frost, G. V., Grosse, G., ... Zona, D. 2016: Pan-Arctic ice-
654 wedge degradation in warming permafrost and its influence on tundra hydrology. *Nature Geoscience*, 9: 312–318,
655 doi: <https://doi.org/10.1038/ngeo2674>.

656 [McCaully, R. E., Arendt, C. A., Newman, B. D., Salmon, V. G., Heikoop, J. M., Wilson, C. J., Sevanto, S., Wales, N.](#)
657 [A., Perkins, G. B., Marina, O. C., and Wullschleger, S. D.: High nitrate variability on an Alaskan permafrost hillslope](#)
658 [dominated by alder shrubs. *The Cryosphere*, 16, 1889–1901. <https://doi.org/10.5194/tc-16-1889-2022>, 2022.](#)
659 [McCaully, R. E., Arendt, C. A., Newman, B. D., Heikoop, J. M., Wilson, C. J., Sevanto, S., ... Wullschleger, S. D. In](#)
660 [Review.: High Temporal and Spatial Nitrate Variability on an Alaskan Hillslope Dominated by Alder Shrubs. *The*](#)
661 [Cryosphere.](#)

662 McClelland, J. W., Holmes, R. M., Peterson, B. J., Raymond, P. A., Striegl, R. G., Zhulidov, A. V., ... Griffin, C. G.
663 2016: Particulate organic carbon and nitrogen export from major Arctic rivers. *Global Biogeochemical Cycles*, 30:
664 629–643, doi: <https://doi.org/10.1002/2015GB005351>.

665 [Mitchell, J. S., and Ruess, R. W. \(2009\). N2 fixing alder \(*Alnus viridis* spp. *fruticosa*\) effects on soil properties across](#)
666 [a secondary successional chronosequence in interior Alaska. *Biogeochemistry* 95, 215–229. doi: 10.1007/s10533-009-](#)
667 [9332-x](#)

668 Mulligan, J. J. 1965: Examination of the Sinuk Iron Deposits Seward Peninsula, Alaska. United States Department of
669 the Interior, 37.

670 Myers-Smith, I. H., Forbes, B. C., Wilmking, M., Hallinger, M., Lantz, T., Blok, D., ... Hik, D. S. 2011: Shrub
671 expansion in tundra ecosystems: dynamics, impacts and research priorities. *Environmental Research Letters*, 6:
672 045509, doi: <https://doi.org/10.1088/1748-9326/6/4/045509>.

673 [Nossov, D. R., Hollingsworth, T. N., Ruess, R. W., and Kielland, K. \(2011\). Development of *Alnus tenuifolia* stands](#)
674 [on an Alaskan floodplain: patterns of recruitment, disease and succession. *J. Ecol.* 99, 621–633. doi: 10.1111/j.1365-](#)
675 [2745.2010.01792.x](#)

676 O'Donnell, J., Douglas, T., Barker, A. and Guo, L., 2021. Changing Biogeochemical Cycles of Organic Carbon,
677 Nitrogen, Phosphorus, and Trace Elements in Arctic Rivers. In *Arctic Hydrology, Permafrost and Ecosystems* (pp.
678 315-348). Springer, Cham.

679 [Patzner, M.S., Kainz, N., Lundin, E., Barczok, M., Smith, C., Herndon, E., Kinsman-Costello, L., Fischer, S., Straub,](#)
680 [D., Kleindienst, S., Kappler, A., Bryce, C., 2022. Seasonal Fluctuations in Iron Cycling in Thawing Permafrost](#)
681 [Peatlands. *Environ. Sci. Technol.* 56, 4620–4631. <https://doi.org/10.1021/acs.est.1c06937>](#)

682 Parkhurst, D., and Appelo, C. A. J. 2013: Description of input and examples for PHREEQC version 3: a computer
683 program for speciation, batch-reaction, one-dimensional transport, and inverse geochemical calculations (USGS
684 Numbered Series No. 6-A43). Reston, VA: U.S. Geological Survey.

685 Perdrial, J. N., Perdrial, N., Vazquez-Ortega, A., Porter, C., Leedy, J., and Chorover, J. 2014: Experimental
686 Assessment of Passive Capillary Wick Sampler Suitability for Inorganic Soil Solution Constituents. *Soil Science*
687 *Society of America Journal*, 78: 486–495, doi: <https://doi.org/10.2136/sssaj2013.07.0279>.

688 Petrone, K. C., Hinzman, L. D., Shibata, H., Jones, J. B., and Boone, R. D. 2007: The influence of fire and permafrost
689 on sub-arctic stream chemistry during storms. *Hydrological Processes*, 21: 423–434, doi:
690 <https://doi.org/10.1002/hyp.6247>.

691 Philben, M., Taş, N., Chen, H., Wullschleger, S. D., Kholodov, A., Graham, D. E., and Gu, B. 2020: Influences of
692 hillslope biogeochemistry on anaerobic soil organic matter decomposition in a tundra watershed. *Journal of*
693 *Geophysical Research: Biogeosciences*, n/a: e2019JG005512, doi: <https://doi.org/10.1029/2019JG005512>.

694 Philben, M., Zheng, J., Bill, M., Heikoop, J. M., Perkins, G., Yang, Z., ... Gu, B. 2019: Stimulation of anaerobic
695 organic matter decomposition by subsurface organic N addition in tundra soils. *Soil Biology and Biochemistry*, 130:
696 195–204, doi: <https://doi.org/10.1016/j.soilbio.2018.12.009>.

697 Prowse, T., Bring, A., Mård, J., and Carmack, E. 2015: Arctic Freshwater Synthesis: Introduction. *Journal of*
698 *Geophysical Research: Biogeosciences*, 120: 2121–2131, doi: <https://doi.org/10.1002/2015JG003127>.

699 Prowse, T., Bring, A., Mård, J., Carmack, E., Holland, M., Instanes, A., ... Wrona, F. J. 2015: Arctic Freshwater
700 Synthesis: Summary of key emerging issues. *Journal of Geophysical Research: Biogeosciences*, 120: 1887–1893, doi:
701 <https://doi.org/10.1002/2015JG003128>.

702 R Core Team. 2020: R: A Language and Environment for Statistical Computing. Vienna, Austria:, R Foundation for
703 Statistical Computing. Retrieved from <https://www.R-project.org/>.

704 [Raudina, Tatiana V., Sergey V. Loiko, Artyom G. Lim, Ivan V. Krickov, Liudmila S. Shirokova, Georgy I. Istigechev,](#)
705 [Daria M. Kuzmina, Sergey P. Kulizhsky, Sergey N. Vorobyev, and Oleg S. Pokrovsky. 2017. “Dissolved Organic](#)
706 [Carbon and Major and Trace Elements in Peat Porewater of Sporadic, Discontinuous, and Continuous Permafrost](#)
707 [Zones of Western Siberia.” *Biogeosciences* 14 \(14\): 3561–84. <https://doi.org/10.5194/bg-14-3561-2017>.](#)

708 [Raynolds, M.K.; Walker, D.A.; Maier, H.A. Plant community-level mapping of arctic Alaska based on the](#)
709 [Circumpolar Arctic Vegetation Map. *Phytocoenologia* 2005, 35, 821–848.](#)

710 [Raynolds, M. K., Walker, D. A., Balseer, A., Bay, C., Campbell, M., Cherosov, M. M., et al. \(2019\). A raster version](#)
711 [of the Circumpolar Arctic Vegetation Map \(CAVM\). Remote Sensing of Environment, 232.](#)
712 <https://doi.org/10.1016/j.rse.2019.111297>

713 Romanovsky, V., Cable, W., and Dolgikh, K. 2020a: Soil Temperature and Moisture, Kougarok Road Mile Marker
714 64, Seward Peninsula, Alaska, beginning 2016 [Data set], doi: <https://doi.org/10.5440/1581586>.

715 Romanovsky, V., Cable, W., and Dolgikh, K. 2020b: Soil Temperature and Moisture, Kougarok Road Mile Marker
716 64, Seward Peninsula, Alaska, beginning 2016 [Data set], doi: <https://doi.org/10.5440/1581586>.

717 Romanovsky, V., Cable, W., and Dolgikh, K. 2020c: Soil Temperature and Moisture, Teller Road Mile Marker 27,
718 Seward Peninsula, Alaska, beginning 2016 [Data set], doi: <https://doi.org/10.5440/1581437>.

719 Romanovsky, V., Cable, W., and Dolgikh, K. 2020d: Soil Temperature and Moisture, Teller Road Mile Marker 27,
720 Seward Peninsula, Alaska, beginning 2016 [Data set], doi: <https://doi.org/10.5440/1581437>.

721 Rowland, J. C., Jones, C. E., Altmann, G., Bryan, R., Crosby, B. T., Hinzman, L. D., ... Geernaert, G. L. 2010: Arctic
722 Landscapes in Transition: Responses to Thawing Permafrost. *Eos, Transactions American Geophysical Union*, 91:
723 229–230, doi: <https://doi.org/10.1029/2010EO260001>.

724 [Ruess, R. W., Anderson, M. D., McFarland, J. M., Kielland, K., Olson, K., and Taylor, D. L. \(2013\). Ecosystem-level](#)
725 [consequences of symbiotic partnerships in an N-fixing shrub from interior Alaskan floodplains. Ecol. Monogr. 83,](#)
726 [177–194. doi: 10.1890/12-0782.1](https://doi.org/10.1890/12-0782.1)

727 Salmon, V. G., Breen, A. L., Kumar, J., Lara, M. J., Thornton, P. E., Wulfschleger, S. D., and Iversen, C. M. 2019:
728 Alder Distribution and Expansion Across a Tundra Hillslope: Implications for Local N Cycling. *Frontiers in Plant*
729 *Science*, 10, doi: <https://doi.org/10.3389/fpls.2019.01099>.

730 Schuur, E. A. G., McGuire, A. D., Schädel, C., Grosse, G., Harden, J. W., Hayes, D. J., ... Vonk, J. E. 2015: Climate
731 change and the permafrost carbon feedback. *Nature*, 520: 171–179, doi: <https://doi.org/10.1038/nature14338>.

732 Shaver, G. R., Billings, W. D., Chapin, F. S., Giblin, A. E., Nadelhoffer, K. J., Oechel, W. C., and Rastetter, E. B.
733 1992: Global Change and the Carbon Balance of Arctic Ecosystems. *BioScience*, 42: 433–441, doi:
734 <https://doi.org/10.2307/1311862>.

735 Shogren, A. J., Zarnetske, J. P., Abbott, B. W., Iannucci, F., Frei, R. J., Griffin, N. A., and Bowden, W. B. 2019:
736 Revealing biogeochemical signatures of Arctic landscapes with river chemistry. *Scientific Reports*, 9: 1–11, doi:
737 <https://doi.org/10.1038/s41598-019-49296-6>.

738 Smith, L. C., Sheng, Y., MacDonald, G. M., and Hinzman, L. D. 2005: Disappearing Arctic Lakes. *Science*, 308:
739 1429–1429, doi: <https://doi.org/10.1126/science.1108142>.

740 Sparks, D. L. 2003: *Environmental soil chemistry* (2nd ed). Amsterdam ; Boston, Academic Press, 352 pp.

741 Spence, C., Kokelj, S., McCluskie, M., and Hedstrom, N. 2015: Impacts of Hydrological and Biogeochemical Process
742 Synchrony Transcend Scale. In *AGU Fall Meeting Abstracts* (Vol. 2015).

743 Sturm, M., Racine, C., and Tape, K. 2001: Increasing shrub abundance in the Arctic. *Nature*, 411: 546–547, doi:
744 <https://doi.org/10.1038/35079180>.

745 [Sulman, B. N., Salmon, V. G., Iversen, C. M., Breen, A. L., Yuan, F., & Thornton, P. E. \(2021\). Integrating arctic](#)
746 [plant functional types in a land surface model using above- and belowground field observations. *Journal of Advances*](#)
747 [in Modeling Earth Systems, 13, e2020MS002396. <https://doi.org/10.1029/2020MS002396>](#)

748 Tape, K. D., Hallinger, M., Welker, J. M., and Ruess, R. W. 2012: Landscape Heterogeneity of Shrub Expansion in
749 Arctic Alaska. *Ecosystems*, 15: 711–724, doi: <https://doi.org/10.1007/s10021-012-9540-4>.

750 Tape, K., Sturm, M., and Racine, C. 2006: The evidence for shrub expansion in Northern Alaska and the Pan-Arctic.
751 *Global Change Biology*, 12: 686–702, doi: <https://doi.org/10.1111/j.1365-2486.2006.01128.x>.

752 Till, A. B., Dumoulin, J. A., Weldon, M. B., and Bleick, H. A. 2011: Bedrock geologic map of the Seward Peninsula,
753 Alaska, and accompanying conodont data. US Department of the Interior, US Geological Survey.

754 Uren, N. C. 2018: Calcium oxalate in soils, its origins and fate – a review. *Soil Research*, 56: 443, doi:
755 <https://doi.org/10.1071/SR17244>.

756 Vonk, J. E., Tank, S. E., Bowden, W. B., Laurion, I., Vincent, W. F., Alekseychik, P., ... Wickland, K. P. 2015:
757 Reviews and syntheses: Effects of permafrost thaw on Arctic aquatic ecosystems. *Biogeosciences*, 12: 7129–7167,
758 doi: <https://doi.org/10.5194/bg-12-7129-2015>.

759 Vonk, J. E., Tank, S. E., and Walvoord, M. A. 2019: Integrating hydrology and biogeochemistry across frozen
760 landscapes. *Nature Communications*, 10: 1–4, doi: <https://doi.org/10.1038/s41467-019-13361-5>.

761 [Walker, D. A., Breen, A. L., Druckenmiller, L. A., Wirth, L. W., Fisher, W., Reynolds, M. K., Sibik, J., Walker, M.](#)
762 [D., Hennekens, S., Boggs, K., Boucher, T., Buchhorn, M., Bultmann, H., Cooper, D. J., Daniels, F. J. A., Davidson,](#)
763 [S. J., Ebersole, J. J., Elmendorf, S. C., Epstein, H. E., Gould, W. A., Hollister, R. D., Iversen, C. M., Jorgenson, M.](#)
764 [T., Kade, A., Lee, M. T., MacKenzie, W. H., Peet, R. K., Peirce, J. L., Schickhoff, U., Sloan, V. L., Talbot, S. S.,](#)
765 [Tweedie, C. E., Villarreal, S., Webber, P. J., and Zona, D.: The Alaska Arctic Vegetation Archive \(AVA-AK\).](#)
766 [Phytocoenologia, 46, 221–229. <https://doi.org/10.1127/phyto/2016/0128.2016>](#)

767 Wallenberger, F. T., and Bingham, P. A. 2009: Fiberglass and Glass Technology: Energy-Friendly Compositions and
768 Applications. Springer Science & Business Media, 479 pp.

769 Walvoord, M. A., and Kurylyk, B. L. 2016: Hydrologic Impacts of Thawing Permafrost—A Review. *Vadose Zone*
770 *Journal*, 15, doi: <https://doi.org/10.2136/vzj2016.01.0010>.

771 Weiss, M., Hobbie, S. E., & Gettel, G. M. (2005). Contrasting Responses of Nitrogen-Fixation in Arctic Lichens to
772 Experimental and Ambient Nitrogen and Phosphorus Availability. *Arctic, Antarctic, and Alpine Research*, 37(3), 396–
773 401. [https://doi.org/10.1657/1523-0430\(2005\)037\[0396:CRONIA\]2.0.CO;2](https://doi.org/10.1657/1523-0430(2005)037[0396:CRONIA]2.0.CO;2)

774 Wilson, C., Bolton, R., Busey, R., Lathrop, E., and Dann, J. 2019: End-of-Winter Snow Depth, Temperature, Density
775 and SWE Measurements at Kougarok Road Site, Seward Peninsula, Alaska, 2018 [Data set], doi:
776 <https://doi.org/10.5440/1593874>.

777 Wilson, C., Bolton, R., Busey, R., Lathrop, E., Dann, J., and Charsley-Groffman, L. 2019: End-of-Winter Snow Depth,
778 Temperature, Density and SWE Measurements at Teller Road Site, Seward Peninsula, Alaska, 2016-2018 [Data set],
779 doi: <https://doi.org/10.5440/1592103>.

780 Wilson, C., Dann, J., Bolton, R., Charsley-Groffman, L., Jafarov, E., Musa, D., and Wulschleger, S. 2021: In Situ
781 Soil Moisture and Thaw Depth Measurements Coincident with Airborne SAR Data Collections, Barrow and Seward
782 Peninsulas, Alaska, 2017 [Data set], doi: <https://doi.org/10.5440/1423892>.

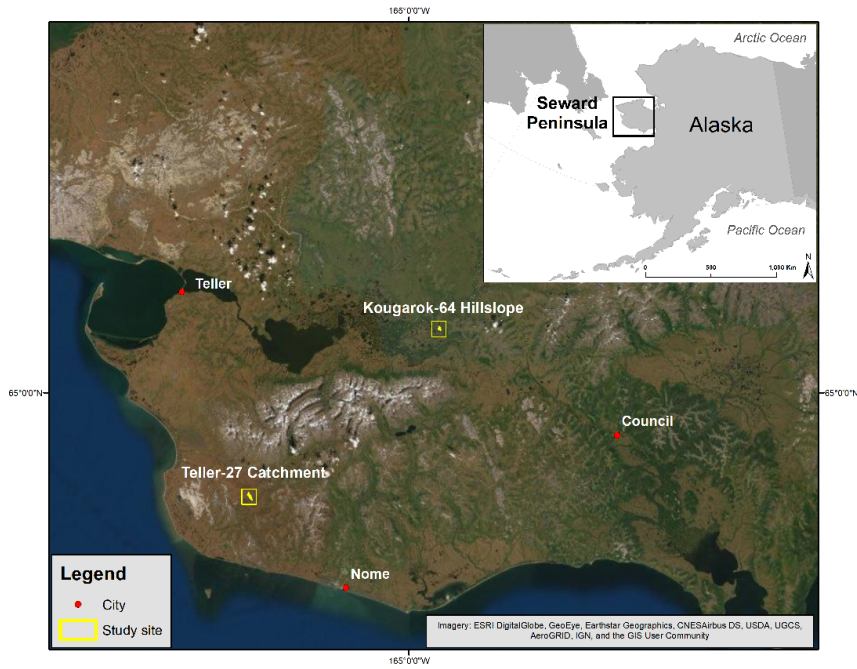
783 Wrona, F. J., Johansson, M., Culp, J. M., Jenkins, A., Mård, J., Myers-Smith, I. H., ... Wookey, P. A. 2016: Transitions
784 in Arctic ecosystems: Ecological implications of a changing hydrological regime. *Journal of Geophysical Research:*
785 *Biogeosciences*, 121: 650–674, doi: <https://doi.org/10.1002/2015JG003133>.

786 [Wulschleger, S. D., Epstein, H. E., Box, E. O., Euskirchen, E. S., Goswami, S., Iversen, C. M., et al. \(2014\). Plant](#)
787 [functional types in earth system models: past experiences and future directions for application of dynamic vegetation](#)
788 [models in high-latitude ecosystems. *Ann. Bot.* 114, 1–16. doi: 10.1093/aob/mcu077](#)

789 Yang, D., Meng, R., Morrison, B. D., McMahon, A., Hantson, W., Hayes, D. J., ... Serbin, S. P. 2020: A Multi-Sensor
790 Unoccupied Aerial System Improves Characterization of Vegetation Composition and Canopy Properties in the Arctic
791 Tundra. *Remote Sensing*, 12: 2638, doi: <https://doi.org/10.3390/rs12162638>.

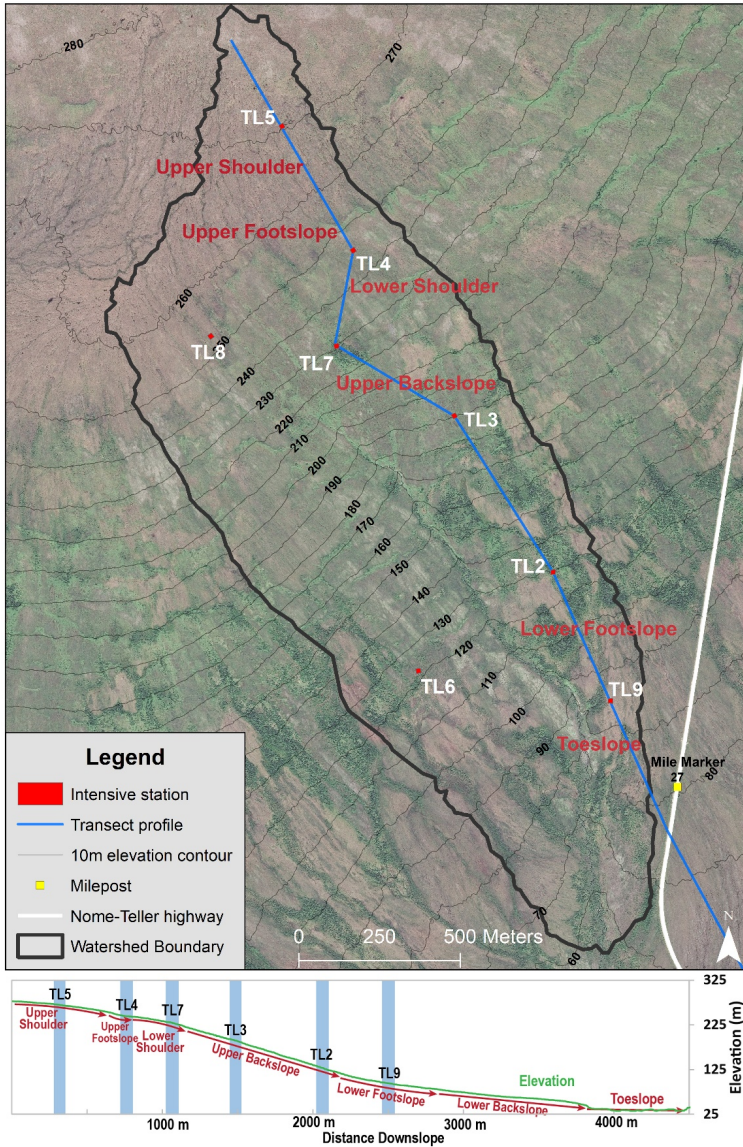
792 [Yang, D., et al. "Landscape-Scale Characterization of Arctic Tundra Vegetation Composition, Structure, and Function](#)
793 [with a Multi-Sensor Unoccupied Aerial System." *Environmental Research Letters* 16 \(8\), 085005 \(2021\).](#)
794 <https://doi.org/10.1088/1748-9326/ac1291>.

795

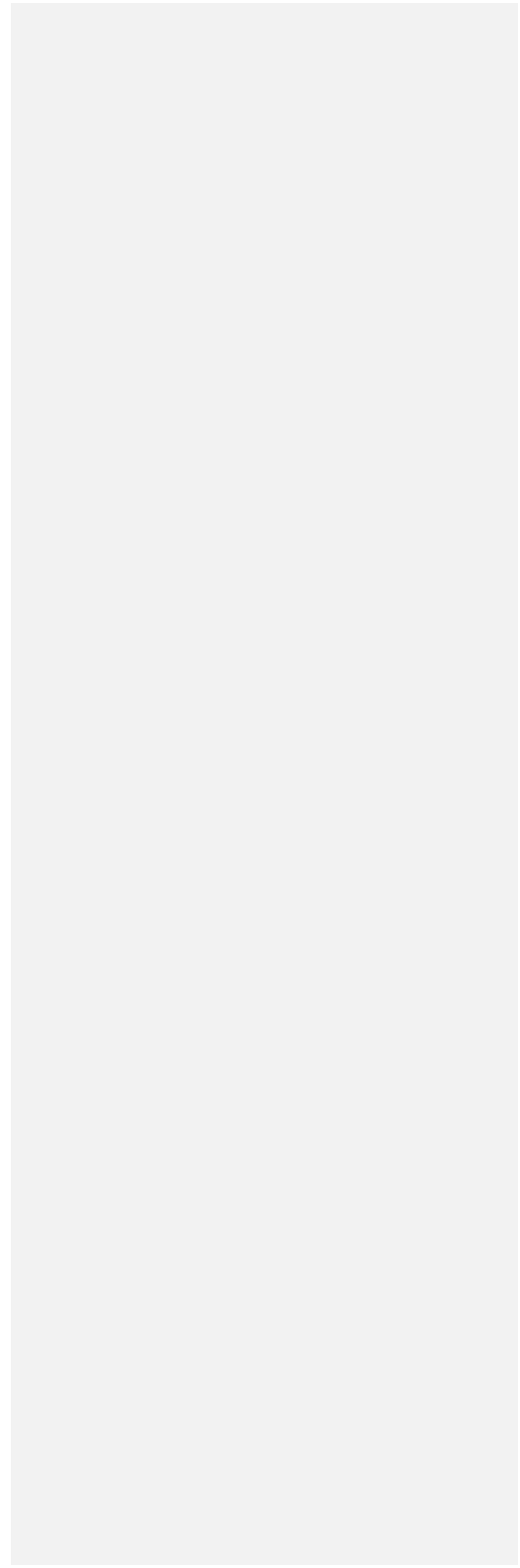


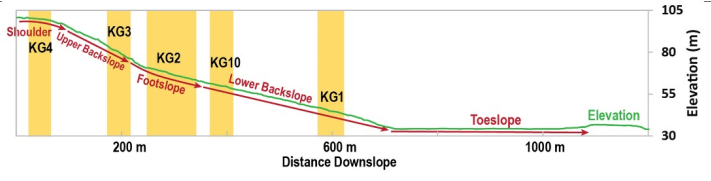
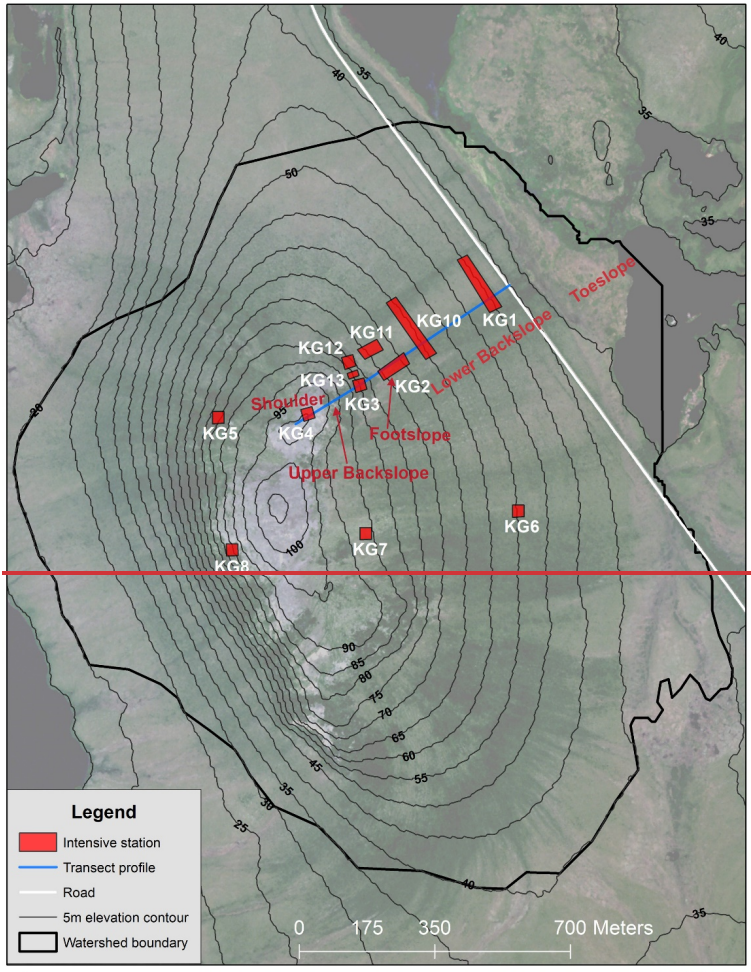
797
798 **Figure 1. Location of the Teller and Kougarak field sites with respect to the municipalities of Teller, Nome, and Council.**
799 **All are located on the Seward Peninsula in northwestern Alaska. RGB composite imagery from the 8-band WorldView-2**
800 **imagery obtained on July 14, 2017 at 1.5 m resolution downloaded from the DigitalGlobe website**
801 **(<https://www.digitalglobe.com/>).**

802
803

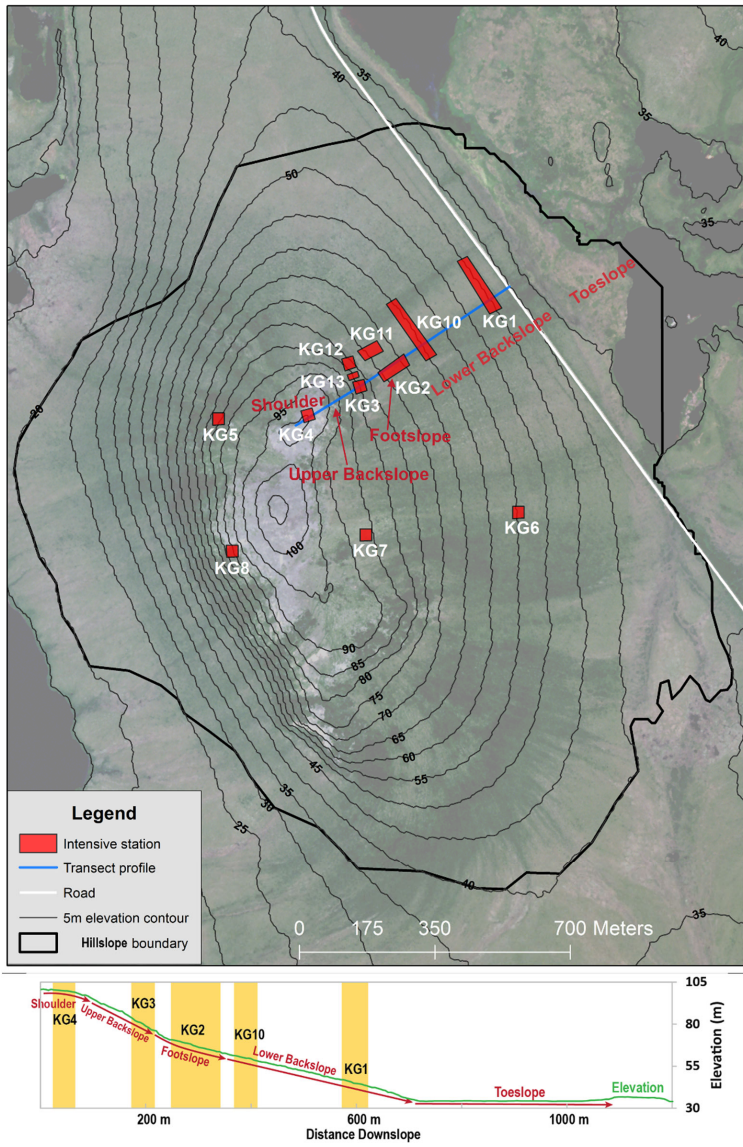


804
 805 Figure 2. Topographic map of Teller. Station areas are shown as red polygons and the topographic station transect is given
 806 as a solid blue line. The hillslope transect elevation profile is given below the map in green, with stations along the transect
 807 in blue and hillslope positions noted with red arrows and text. RGB composite imagery from the 8-band WorldView-2
 808 imagery obtained on July 27, 2011 at 1.5 m resolution downloaded from the DigitalGlobe website
 809 (<https://www.digitalglobe.com/>).



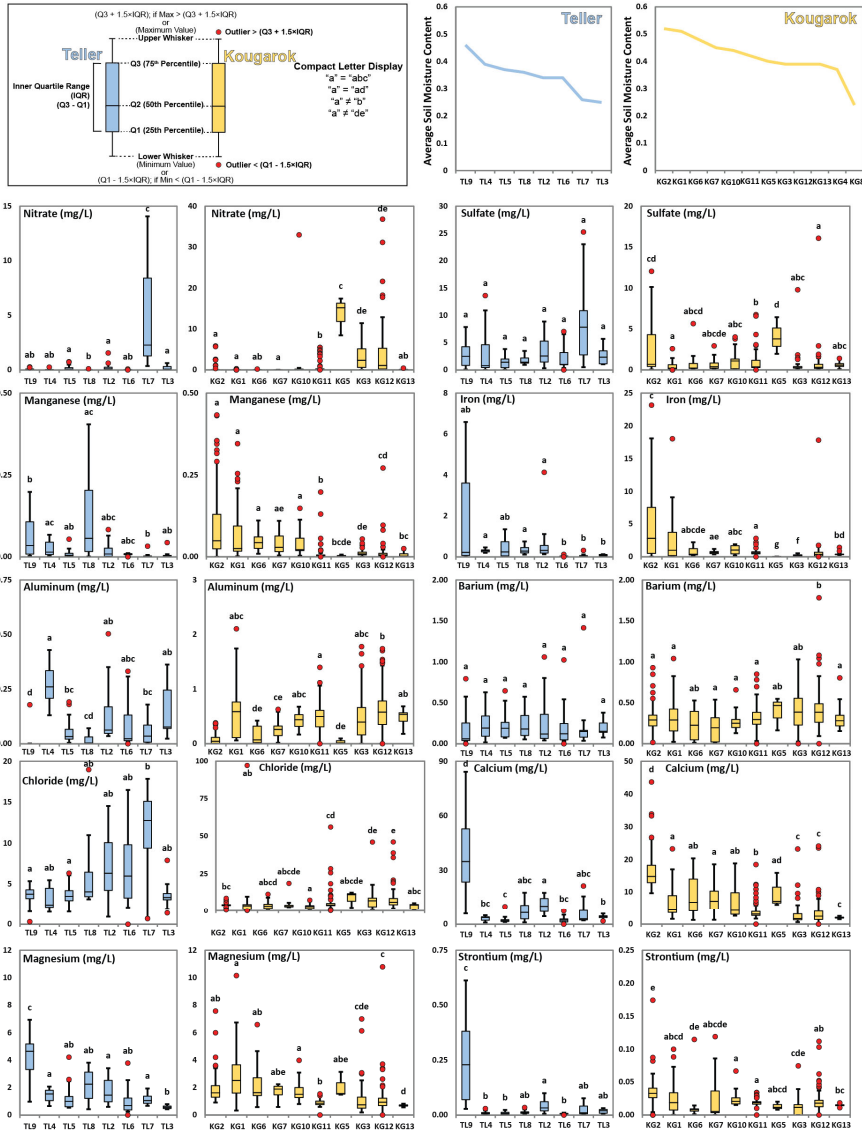


811



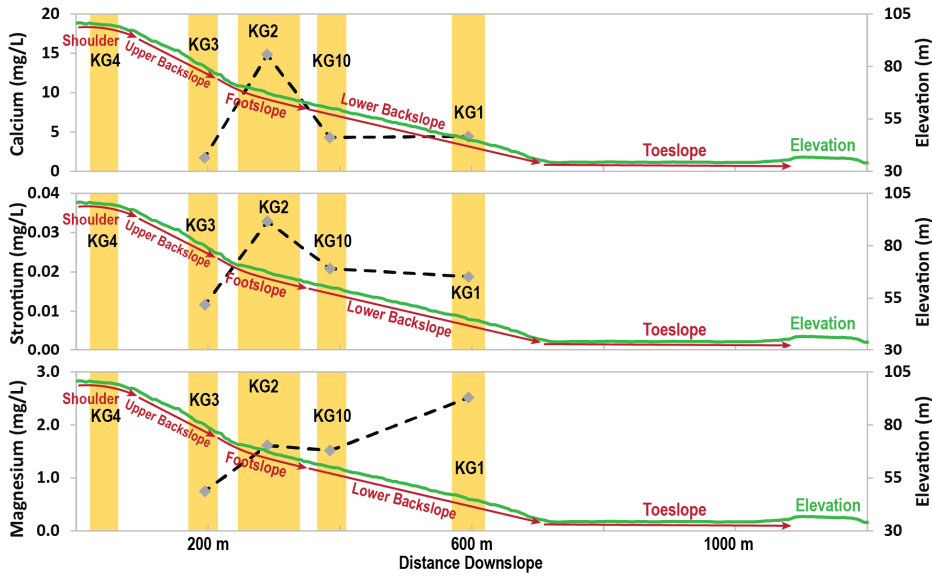
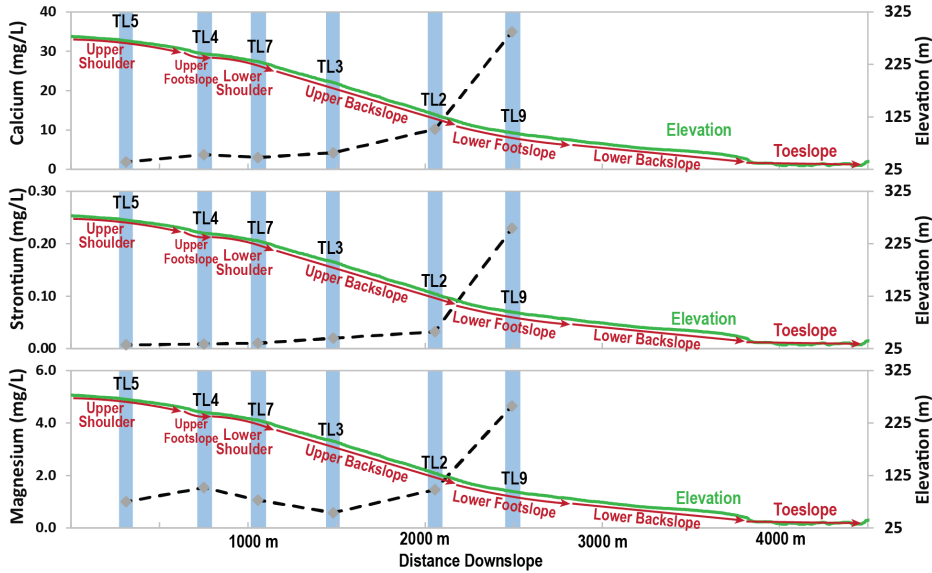
812

813 Figure 3. Topographic map of Kougarok. Station areas are shown as red polygons and the station transect is given as a
 814 solid blue line. The transect elevation profile is given below the map in green, with stations along the transect in yellow and
 815 hillslope positions noted with red arrows and text. RGB composite imagery from the 8-band WorldView-2 imagery obtained
 816 on July 14, 2017 at 1.5 m resolution downloaded from the DigitalGlobe website (<https://www.digitalglobe.com/>).



818
 819 **Figure 4.** Mean COI concentrations at Teller (blue) and Kougarok (yellow) stations. Stations are arranged (left to right) by
 820 soil moisture content determined by P-Band SAR (top right). Boxplots show the first, second, and third quartiles, with
 821 box whiskers representing either 150% of the inner quartile range (IQR), or the maximum or minimum value, when that
 822 value was less than 1.5×IQR. Red circles represent data points outside of the 1.5×IQR whiskers (i.e. outliers). Note that the
 823 concentration scales on the Teller and Kougarok plots often differ.

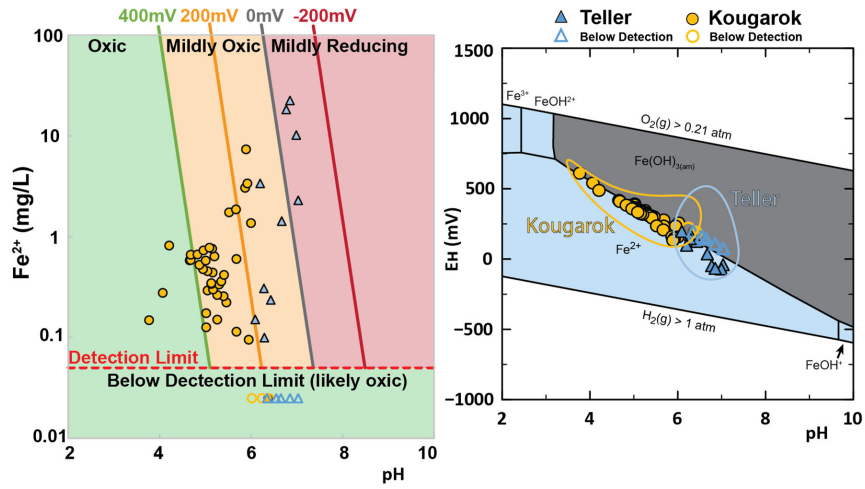
824



825

826 Figure 5. Median (50th percentile) concentrations (grey diamonds with dashed black lines) of Ca, Sr, and Mg, with distance
 827 downslope at Teller (blue) and Kougarak (yellow) along topographic transects; areas of stations are indicated by blue and
 828 yellow colouring, respectively. The elevation profiles of the hillslopes are plotted in green, on separate y-axes (right axes).
 829 Topographic regions of both catchments are indicated by red arrows along the elevation gradient.

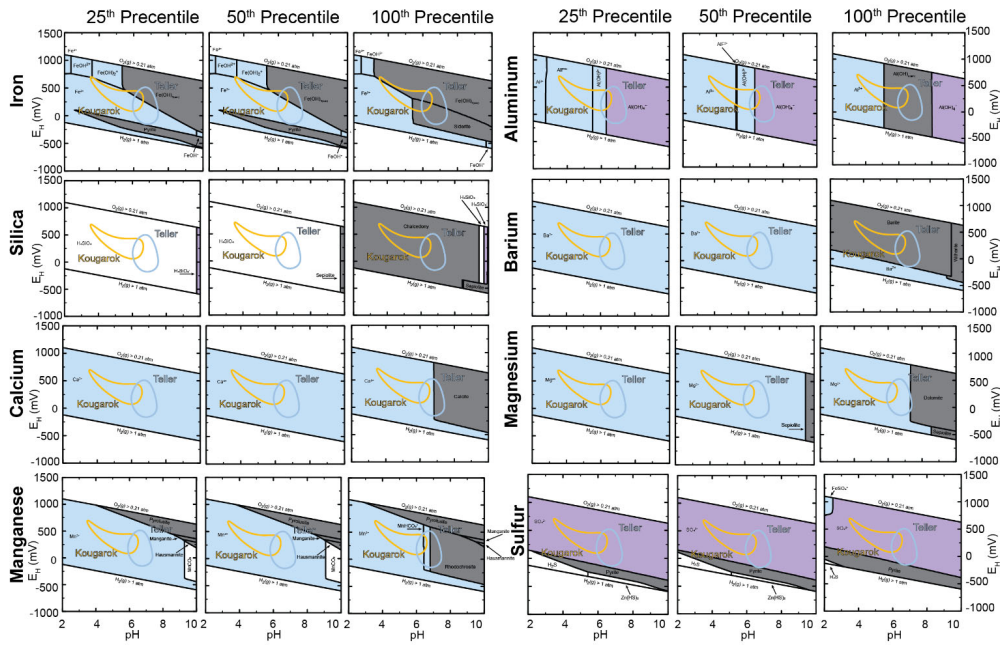
830



831

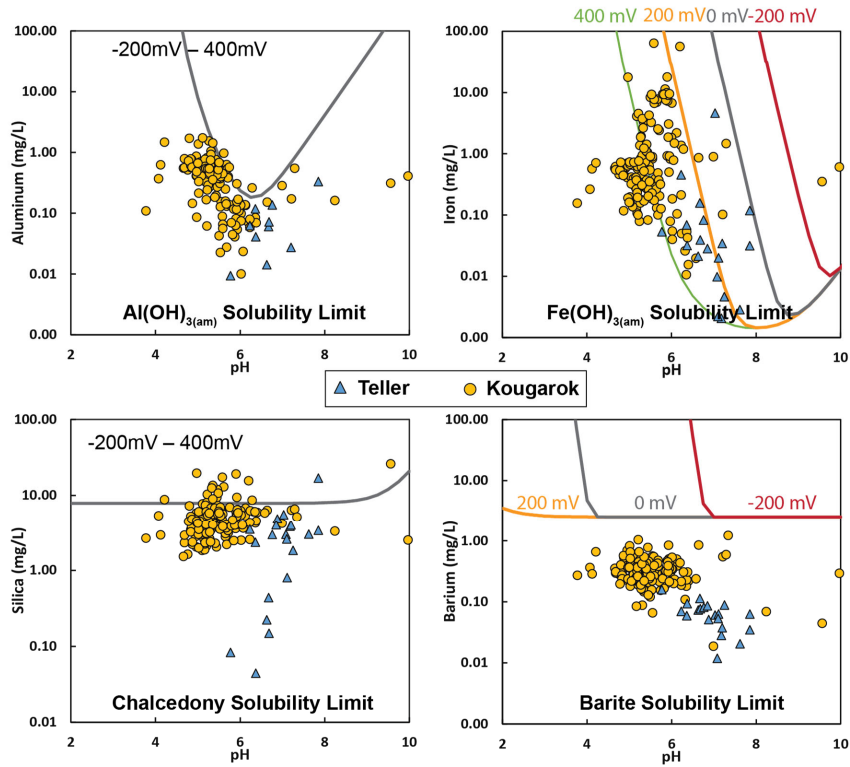
832 Figure 6. Left: Model-predicted Fe²⁺ concentrations in saturated solutions of Fe(OH)_{3(am)} at fixed E_H conditions of 400 mV
833 (green), 200 mV (orange), 0 mV (grey), and -200 mV (red), compared with field concentrations of Fe²⁺ at Teller (red circles)
834 and Kougarok (yellow circles). Right: Fe predominance diagram, showing the dominant specie of Fe under a range of
835 Eh/pH conditions. Eh/pH regions relevant to Teller and Kougarok are outlined in blue and yellow, respectively. Samples
836 with Fe²⁺ concentrations below the detection limit are given as colour coordinated open circles set at 0.025 mg·L⁻¹ (half the
837 detection limit) in both sides of the figure.

838



839
 840 Figure 7. E_H/pH diagrams for key species that indicated possible mineral formation under the E_H/pH conditions present at
 841 either Teller or Kougarak. The E_H and pH conditions observed at Teller and Kougarak are overlaid as blue and yellow
 842 lines, respectively. Mineral species (solids) are shown in grey, cations are shown in blue, anions are shown in purple,
 843 neutral species are shown in white. Predominance diagrams were created in PhreePlot using the phreeqc.dat database, with
 844 inorganic carbonate reduction to methane “turned off.”

845



846

847

848

Figure 8. Modelled solute concentrations in solutions saturated with $\text{Al}(\text{OH})_{3(\text{am})}$, $\text{Fe}(\text{OH})_{3(\text{am})}$, chalcedony, and barite, with respect to pH (x-axis) and E_H (model lines), overlaid with observed solute concentrations.

849

850 **240. Tables**

851 **Table 1. Teller Station Physical Characteristics**

	Hillslope Position	Vegetation				Relative wetness			Permafrost			
		Vegetation type	Average (maximum) canopy height (cm)	Dominant PFT	Low to tall shrub cover	Average TDR soil moisture (VMC)	Average P-band SAR (VMC)	Average snow depth (cm)	Average Ground Temperature (°C)	Permafrost Extent	Average (maximum) thaw depth (cm)	
TL9	Lower Foothslope		2834 (41)	Graminoid Bryophyte	44%	10%	NA	0.46	68.4	0	Marginal	101 (>20)
TL5	Upper Shoulder	Wetland complex	1234 (45)	Graminoid	45%	7%	0.55	0.37	103.3	-0.45	Near-surface	97' (>114')
TL8	Upper Foothslope		47 (34)	Bryophyte	33%	20%	0.55	0.36	77.7	-0.6		69' (>120)
TL3	Upper Backslope	Cassiope dwarf shrub	913 (23)	Evergreen dwarf shrub	47%	124%	NA	0.25	62.1	2.2	None/ deep	72' (82')
TL4	Upper Foothslope	tundra	408 (14)		58%	4%	0.35	0.39	89.5	0.5	Marginal	40' (70')
TL2	Upper Backslope	Mesic willow shrubland	8432 (141)	Deciduous low to tall shrub (willow)	44%	44%	0.4	0.34	124	2.4	None/ deep	75' (>120)
TL7	Lower Shoulder		468-151 (189)		37%	37%	0.46	0.26	128.8	2.4		51' (66')
TL6	Upper Backslope	Willow-birch tundra	7464 (115)	ForbDeciduous-low shrub (willow & birch)	23%	32%	0.38	0.34	86.4	1.2	None/ deep	67' (102')

Formatted Table

852

853 PFT – plant functional type; dwarf shrub (height <40 cm), low shrub (height 40-200 cm), low to tall shrub (height 40 to >200 cm tall).
 854 Deciduous shrub PFT classes identify the dominant species in the plant community as either willow or willow and birch. There is no alder at
 855 the Teller site. Low to tall shrub cover represents the sum of deciduous low shrubs, deciduous low to potentially tall willow and birch, and
 856 deciduous low to tall alder.

857 ¹Single point soil moisture measurements. Data are more accurate than P-band SAR but represent a much smaller spatial scale.

858 ²P-band SAR has 30m resolution.

859 ³Resistive layer was rock; all others are permafrost. A temperature probe was used to determine if the resistive layer was permafrost (≤0 °C)
 860 or rock (>2 °C). Thaw depth is an average of 4 measurements from the vegetation plot corners within the IS and was measured at the end of
 861 the growing season.
 862

863 **Table 2. Kougarok Station Physical Characteristics**

	Hillslope Position	Vegetation				Relative wetness			Permafrost			
		Vegetation type	Average (maximum) canopy height (cm)	Dominant PFT		Low to tall shrub cover	Average TDR soil moisture (VMC)	Average P-band SAR (VMC)	Average snow depth (cm)	Average Ground Temperature (°C)	Permafrost Extent	Average (maximum) thaw depth (cm)
KG3	Upper Backslope	Alder shrubland	204 (265)	Deciduous low to tall shrub (alder)	30%	53% ¹	0.19	0.39	131.3	-0.01	Near-surface	48 [†] (53 [†])
KG12	Footslope		NA	NA	NA	NA	0.30*	0.39	NA	NA		NA*
KG1	Lower Backslope		60 (90)	Deciduous low shrub (alder, willow & birch)	31%	44% ¹	NA	0.51	83.4	-2.5		61 (68)
KG2	Footslope	Alder savanna in tussock tundra	48 (73)	Graminoid	30%	42% ¹	0.63	0.52	102.3	-1.2	Near-surface	75 (89)
KG6	Lower Backslope		24 (61)	Graminoid	46%	17% ¹	0.36	0.48	66.2	-2.2		58 (62)
KG10	Lower Backslope		NA	NA	NA	NA	NA*	0.44	71.4	NA		NA*
KG11	Footslope		NA	NA	NA	NA	0.59*	0.42	NA	NA		NA*
KG7	Upper Backslope	Tussock-lichen tundra	20 (22)	Graminoid	34%	14% ¹	0.51	0.45	54.7	-2.1	Near-surface	76 (100)
KG4	Shoulder	Dryas-lichen shrub tundra	6 (12)	Evergreen dwarf shrub	62%	1% ¹	NA	0.37	NA	-1.9	Near-surface	0 [†] (0 [†])
KG13	Upper Backslope		NA	NA	NA	NA	0.41*	0.39	92.1	NA		NA*
KG5	Upper Backslope	Willow-birch tundra	62 (137)	Deciduous low shrub (willow & birch)	60%	62% ¹	NA	0.4	178.4	> 0	Deep	88 (96)
KG8	Upper Backslope		45 (120)	Evergreen dwarf shrub	52%	42% ¹	0.23	0.24	85.5	-0.04	Near-surface	44 [†] (58 [†])

Formatted: Centered

Formatted Table

Formatted: Centered

Formatted Table

Formatted: Centered

Formatted: Centered

Formatted Table

Formatted: Centered

Formatted Table

Formatted: Centered

Formatted Table

864
 865 Note: PFT – plant functional type. Deciduous shrub PFT classes identify the dominant species in the community as either willow, alder,
 866 willow and birch, or alder, willow, and birch. Low to tall shrub cover represents the sum of deciduous low shrubs, deciduous low to potentially
 867 tall willow and birch, and deciduous low to tall alder.
 868 ¹Single point soil moisture measurements. Data are more accurate than P-band SAR but represent a much smaller spatial scale.
 869 ²P-band SAR has 30m resolution.
 870 *Average gravimetric water content measurements, corrected to VMC by bulk density.
 871 [†]Resistive layer was rock; all others are permafrost. A temperature probe was used to determine if the resistive layer was permafrost (≤ 0 °C)
 872 or rock (>2 °C). Thaw depth is an average of 4 measurements from the vegetation plot corners within the 1S and was measured at the end of
 873 the growing season.

875 Table 3. Inter-Site Mann-Whitney U-Test Results

	Teller			Kougarok			z	Site with Higher Median	Effect Size	Difference in Correlation
	n	$\sum R_i$	U_i	n	$\sum R_i$	U_i				
Na	59	3184	14811.5	275	52761.5	1413.5	9.95	Kougarok	0.54	large
F	59	3502	14375.5	273	51776.5	1731.5	9.46	Kougarok	0.52	large
K	59	3882	14113	275	52063	2112	8.92	Kougarok	0.49	medium-large
Si	59	4119	13876.5	275	51826.5	2348.5	8.56	Kougarok	0.47	medium-large
Al	58	4952	12709	275	50659	3241	7.11	Kougarok	0.39	medium
Oxalate	57	4996	12161.5	272	49289.5	3342.5	6.75	Kougarok	0.37	medium
B	59	5429	12566.5	275	50516.5	3658.5	6.62	Kougarok	0.36	medium
Zn	58	5605	12056	275	50006	3894	6.12	Kougarok	0.34	medium
SO ₄	58	13653	3892.5	273	41293.5	11941.5	6.08	Teller	0.33	medium
Fe	58	5958	11703	275	49653	4247	5.60	Kougarok	0.31	medium
Ba	58	6256	11405.5	275	49355.5	4544.5	5.15	Kougarok	0.28	medium
Ti	58	6266	11395.5	275	49345.5	4554.5	5.13	Kougarok	0.28	medium
NO ₂	54	5588	10585.5	272	47713.5	4102.5	5.12	Kougarok	0.28	medium
Li	58	7778	9883	275	47833	6067	2.86	Kougarok	0.16	small-medium
Br	58	8485	9060.5	273	46461.5	6773.5	1.73	Equal	0.09	small
NO ₃	58	8576	8969	273	46370	6865	1.59	Kougarok	0.09	small
Sr	58	8683	8978	275	46928	6972	1.51	Kougarok	0.08	small
PO ₄	54	9659	6460.5	271	43316.5	8173.5	1.36	Equal	0.08	small
Mg	58	10495	7166	275	45116	8784	1.21	Teller	0.07	small
Cr	58	8884	8777	275	46727	7173	1.20	Kougarok	0.07	small
Mn	58	9164	8497	275	46447	7453	0.78	Teller	0.04	small
Cl	58	9221	8266.5	272	45394.5	7509.5	0.57	Kougarok	0.03	small
Ca	58	10016	7645	275	45595	8305	0.50	Teller	0.03	small

Table 4. Dominant Environmental Controls on SPW Geochemistry at Teller and Kougarok

Environmental Control	Analytes Affected
Vegetation	NO₃NO₂⁻
Soil Moisture/Redox	NO₃NO₂⁻ , Mn, Fe, SO ₄ (occasionally)
Water/Soil Interactions & Hydrologic Transport	Ca, Mg, Sr
Mineral Solubility	Al, Ba, Si, Fe

Formatted: Subscript

Formatted: Subscript